Published for SISSA by Springer

Received: June 19, 2025
Revised: September 17, 2025
Accepted: October 24, 2025
Published: November 26, 2025

Search for the lepton-flavour-violating decays $B^0 \to K^{*0}\tau^{\pm}e^{\mp}$

The LHCb collaboration

E-mail: tommaso.fulghesu@cern.ch

Abstract: A first search at LHCb for the lepton-flavour-violating decays $B^0 \to K^{*0}\tau^{\pm}e^{\mp}$ is presented. The analysis is performed using a sample of proton-proton collision data, collected with the LHCb detector at a centre-of-mass energy of 13 TeV between 2016 and 2018, corresponding to an integrated luminosity of $5.4\,\text{fb}^{-1}$. No significant signal is observed, and upper limits on the branching fractions are determined to be $\mathcal{B}(B^0 \to K^{*0}\tau^{-}e^{+}) < 5.9\ (7.1) \times 10^{-6}$ and $\mathcal{B}(B^0 \to K^{*0}\tau^{+}e^{-}) < 4.9\ (5.9) \times 10^{-6}$ at the 90% (95%) confidence level. These results correspond to the current most stringent upper limits for $b \to s\tau l$ transitions.

Keywords: B Physics, Beyond Standard Model, Hadron-Hadron Scattering, Rare Decay

ArXiv ePrint: 2506.15347

https://doi.org/10.1007/JHEP11(2025)172

JHEP11(2025)172

Contents

JHEP11(2025)172

1 Introduction

Lepton-flavour violation (LFV) has been observed in neutral leptons through neutrino oscillations [1–8]. For charged leptons, however, the Standard Model (SM) predicts that LFV is beyond any current experimental sensitivity [9]. Thus, any observation of a charged LFV decay would provide clear evidence for physics beyond the SM.

The LHCb collaboration has performed searches for lepton-flavour-violating b-hadron decays into final states with an electron and a muon [10–12], and with a tau and a muon [13–16]. No searches at LHCb have been conducted involving a tau and an electron. Analogous searches have been performed by other experiments, finding no signal [17–25]. The most stringent limit on the rate of a $b \to s\tau e$ transition is $\mathcal{B}(B^+ \to K^+\tau^\pm e^\mp) < 1.5 \times 10^{-5}$ at the 90% confidence level, set by the Belle collaboration [24]. For the decay $B^0 \to K^*(892)^0\tau^\pm e^\mp$, an upper limit is set by the Belle collaboration to $\mathcal{B}(B^0 \to K^{*0}\tau^- e^+) < 4.4 \times 10^{-5}$ and $\mathcal{B}(B^0 \to K^{*0}\tau^+ e^-) < 2.8 \times 10^{-5}$ at the 90% confidence level [26]. In this article, the search for the charged lepton-flavour-violating decay $B^0 \to K^*(892)^0\tau^\pm e^\mp$ at LHCb is presented. The inclusion of charge-conjugate processes is implied throughout. The $K^*(892)^0$ (referred to in the text as K^{*0}) meson is reconstructed through its decay into a kaon and a pion. The

decays $B^0 \to K^{*0}\tau^+e^-$ with the charged kaon and the electron having opposite charges and $B^0 \to K^{*0}\tau^-e^+$ with the charged kaon and the electron having the same charge are treated independently. These channels could be affected differently by extensions beyond the SM [27], and they are contaminated by different background contributions. The τ lepton is reconstructed through the decays $\tau^- \to \pi^-\pi^+\pi^-\nu_\tau$ or $\tau^- \to \pi^-\pi^+\pi^-\pi^0\nu_\tau$ for which the π^0 meson is not explicitly reconstructed, representing a combined branching ratio of approximately 14%. The decay $B^0 \to D^-D_s^+$ followed by $D^- \to K^+\pi^-\pi^-$ and $D_s^+ \to K^+K^-\pi^+$, sharing six tracks in the final states and with a precisely known branching fraction, is used both as a normalisation and control channel to test the reliability of the simulation and to evaluate the relevant systematic uncertainties.

This analysis is performed on a dataset of proton-proton (pp) collisions collected with the LHCb detector at a centre-of-mass energy of 13 TeV between 2016 and 2018, corresponding to an integrated luminosity of 5.4 fb^{-1}. In order to avoid experimenter's bias, the results of the analysis were not examined until the full procedure had been finalised.

2 LHCb detector, trigger and simulation

The LHCb detector [28, 29] is a single-arm forward spectrometer covering the pseudorapidity $2 < \eta < 5$, designed for the study of particles containing b or c quarks. The detector includes a high-precision charged-particle reconstruction (tracking) system consisting of a silicon-strip vertex detector surrounding the pp interaction region [30], a large-area silicon-strip detector located upstream of a dipole magnet with a bending power of about 4 T m, and three stations of silicon-strip detectors and straw drift tubes [31, 32] placed downstream of the magnet. The tracking system provides a measurement of the momentum, p, of charged particles with a relative uncertainty that varies from 0.5% at low momentum to 1.0% at 200 GeV/c. The minimum distance of a track to a primary vertex (PV), the impact parameter (IP), is measured with a resolution of $(15 + 29/p_{\text{T}})$ µm, where p_{T} is the component of the momentum transverse to the beam, in GeV/c. Different types of charged hadrons are distinguished from one another using information from two ring-imaging Cherenkov (RICH) detectors [33]. Photons, electrons and hadrons are identified by a calorimeter system consisting of scintillating-pad and preshower detectors, an electromagnetic (ECAL) and a hadronic calorimeter. Muons are identified by a system composed of alternating layers of iron and multiwire proportional chambers [34].

The online event selection is performed by a trigger [35, 36], consisting of a hardware stage, based on information from the calorimeter and muon systems, followed by a software stage, which performs full event reconstruction. In the hardware stage, selected events are required to have at least one high-p_{T} electron, muon or hadron. In this analysis, signal candidates belong to three mutually exclusive categories depending on whether the events were selected by: a high-energy electron from the signal candidate (eTOS); a reconstructed particle not belonging to the signal candidate (TIS); a reconstructed hadron from the signal candidate (hTOS).[1] Candidates in each category should not satisfy the requirements of the previous ones. The software trigger is organised in two stages. The first requires a two-track secondary vertex with a significant displacement from any PV, and at least one charged

[1]TOS: Trigger On Signal, TIS: Trigger Independent of Signal.

JHEP11(2025)172

particle with a minimum requirement on the transverse momentum that is also inconsistent with originating from a PV. The second stage is based on a multivariate algorithm [37, 38] exploiting kinematic, geometric, and lepton-identification criteria to select events containing secondary vertices consistent with the decay of a b hadron.

Simulation is used to optimise the selection, determine the signal model for the fit and obtain the selection efficiencies. In the simulation, pp collisions are generated using Pythia 8 [39] with a specific LHCb configuration [40]. The B^0 decay is assumed to proceed according to a phase-space distribution in the kinematic space. The τ decay is simulated using a dedicated model tuned with BaBar data [41] from the Tauola decay library [42], while the decays of all other unstable particles are described by EvtGen [43], in which final-state radiation is generated using Photos [44]. Finally, the interaction of the generated particles with the detector, and its response, are implemented using the Geant4 toolkit [45, 46] as described in ref. [47].

3 Signal candidate mass reconstruction

Neutrinos from the τ decay are not reconstructed since they do not interact with the detector. In addition, the π^0 meson from the $\tau^- \to \pi^-\pi^+\pi^-\pi^0\nu_\tau$ decay is ignored during the reconstruction. Hence, the invariant mass of the six tracks in the final state, $m(K^{*0}\tau e)$, peaks at a value lower than the true B^0 meson mass and exhibits degraded resolution [48]. Consequently, the $m(K^{*0}\tau e)$ variable is poorly suited to separate signal from background. Instead, the B^0 mass is calculated from the outcome of a kinematic fit in which the entire decay chain is reconstructed imposing the following constraints [49]: the three charged pions from the tau decay must form a vertex; the missing momentum in the decay chain is attributed to a massless neutrino originating from the τ-decay vertex; the mass of the τ candidate is constrained to the known τ mass [48]; the τ candidate must originate from the B^0 decay vertex, which is reconstructed using the charged kaon and pion from the K^{*0} decay, along with the electron. The resulting reconstructed B^0 mass, denoted $m_{\rm fit}$, has a largely improved resolution, as shown in figure 1 for simulated events, and is therefore used in this analysis.

In addition, the electron might emit bremsstrahlung while travelling through the detector. In case this occurs upstream of the magnet, the electron momentum is underestimated and the photons and electron energies are deposited in different calorimeter cells. A dedicated procedure searches for energy deposits with transverse energy $E_{\rm T} > 75\,\text{MeV}$, not associated with charged tracks, within a region of the ECAL defined by the extrapolation of the electron track upstream of the magnet. Such "bremsstrahlung clusters" are added to the measured electron momentum, improving its determination. The procedure is limited by the energy threshold of the clusters, the acceptance and resolution of the calorimeter, and by the presence of energy deposits wrongly interpreted as bremsstrahlung clusters. The bremsstrahlung further worsens the mass resolution, though its impact is less than that due to the missing neutrino in the τ decay. It is taken into account by modelling the signal shape differently for candidates where bremsstrahlung photons have been added.

JHEP11(2025)172

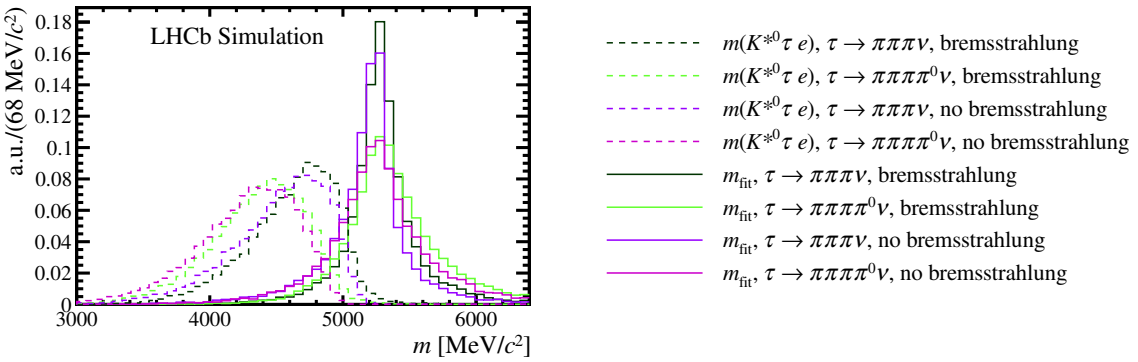

Figure 1. Comparison in simulated signal candidates between (dashed lines) the mass $m(K^{*0}\tau e)$, corresponding to the invariant mass of the tracks in the final state, and (bold lines) the mass $m_{\rm fit}$ accounting for the missing momentum carried from the neutrino via a decay chain fit with kinematic constraints. Legends with the various components of the signal are shown next to the plot.

4 Signal candidate selection

Candidate $B^0 \to K^{*0}\tau^{\pm}e^{\mp}$ decays are reconstructed by combining six charged tracks with $2.0 < \eta < 4.9$. Five tracks are required to have $p < 110\,\text{GeV}/c$ and $p_{\rm T} > 250\,\text{MeV}/c$. A sixth track, with $3 < p < 110\,\text{GeV}/c$ and $p_{\rm T} > 500\,\text{MeV}/c$ should be within the calorimeter acceptance and satisfy loose electron-identification requirements. Candidate K^{*0} mesons are reconstructed by combining two tracks of opposite charge, one compatible with a kaon hypothesis and the other with a pion hypothesis. Those satisfying an invariant mass within $700 < m(K^{*0}) < 1100\,\text{MeV}/c^2$ undergo a kinematic fit procedure to determine its vertex. The other three remaining tracks, each identified as pions, with momentum $p > 2\,\text{GeV}/c$, should originate from another vertex. These pions form the τ candidate, with a charge opposite to that of the electron and with a reconstructed invariant mass $0.5 < m(\tau) < 2.0\,\text{GeV}/c^2$. The τ vertex must have a radial distance between 0.1 and 7.0 mm and a distance along the z-axis, pointing along the beam axis, larger than 5.0 mm. Distances are evaluated with respect to the PV associated to the B candidate.

The K^{*0} and τ candidates are required to have a transverse momentum $p_{\rm T} > 1\,\text{GeV}/c$. Together with the electron, they form a B^0 candidate, with a decay vertex sufficiently displaced from any PV. Finally, the $K^{*0}\tau$ invariant mass is required to be lower than $5\,\text{GeV}/c^2$ and the reconstructed B^0 candidate mass $2 < m(K^{*0}\tau e) < 10\,\text{GeV}/c^2$. A sample of data with τ and electron of the same charge (referred to as the same-sign sample in the following) is also selected as a proxy for backgrounds.

Background contributions can be divided into two categories: combinatorial background, arising from random combinations of tracks; and physics background, due to b-hadron decays partially reconstructed and/or reconstructed with misidentified particles. In particular, a large component of the background involves D mesons with a decay time compatible with that of the τ lepton and decaying into multiple charged tracks. To optimise the rejection of these backgrounds of a different nature, a multistage selection procedure is used. The procedure is carried out without involving candidates in the region where the signal is expected, referred to as the signal region and defined as $4.6 < m_{\rm fit} < 6.4\,\text{GeV}/c^2$. The

JHEP11(2025)172

region $6.4 < m_{\rm fit} < 12.0\,{\rm GeV}/c^2$ is referred to as the upper mass sideband, while the region $2.0 < m_{\rm fit} < 4.6\,{\rm GeV}/c^2$ as the lower mass sideband. The former is dominated by combinatorial background, while the latter contains both combinatorial and physics background.

The Punzi figure of merit [50], defined as $\varepsilon/(\sigma/2+\sqrt{Y_{\rm b}})$ with $\sigma = 3$, is used to optimise the threshold requirement for each selection stage, apart from specific vetoes discussed later. Here, ε is the efficiency of the signal selection, obtained from simulation, and Y_b is the background yield in the signal region, estimated differently for each selection stage.

The first stage of the selection is based on a multivariate discriminant exploiting the differences between the topologies of the signal decays and the combinatorial background. A gradient-boosted decision tree (GBDT) algorithm [51] implemented in the TMVA package [52] combines information from: the vertex-fit χ^2 of the B^0 and τ candidates; the B^0 and K^{*0} flight distances; the χ^2 of the flight distances of the B^0, K^{*0} and the τ candidates; and the B^0 impact parameter. The B^0 flight distance is evaluated with respect to the PV, while that of the K^{*0} and τ are evaluated with respect to the B^0 vertex. The classifier is trained using simulated samples as a signal proxy and the upper mass sideband of the opposite-sign data sample as a background proxy. A k-folding approach [53] is used to exploit the training samples without biasing the output of the classifier. For the threshold optimisation, the background yield in the signal region is extrapolated from a fit to the $m_{\rm fit}$ distribution of the B^0 candidates in sidebands, modelled by a gamma function. The obtained background yield is then corrected to account for possible extrapolation biases by a fit to the same-sign sample in the signal region.

A particle selected from a partially reconstructed decay is often surrounded by other particles that are not used to reconstruct the candidate. To exploit this feature, the second stage of the selection makes use of a Fisher discriminant [54], built using the k-folding procedure and based on the following variables evaluating the particle isolation: the logarithm of the smallest variation of the B^0 vertex-fit χ^2 when adding one or two tracks independently; the invariant mass of the B^0 candidate and of the additional track giving the smallest variation to the B^0 vertex-fit χ^2; the invariant mass of the K^{*0} or τ candidate and of the two additional tracks giving the smallest variation to the K^{*0} or τ vertex-fit χ^2; the number of tracks that modify the vertex-fit χ^2 by less than 9 units if added to the K^{*0} vertex; the asymmetry of the transverse momentum of all charged tracks (or, separately, neutral particles) in a cone with aperture $\Delta R = \sqrt{\Delta\phi^2 + \Delta\eta^2} = 0.4$ around the K^{*0} or τ direction, where ϕ is the polar angle. The Fisher discriminant is chosen for its stability in the training procedure, despite the small size of the training samples available at this point in the selection. Signal simulation and, for the background, same-sign data that fall into the signal mass region are used for training and optimisation of the threshold. The input variables used in both classifiers are validated by checking the agreement between data and simulation on the $B^0 \to D^- D_s^+$ sample.

The third stage makes use of the multivariate selection dedicated to the rejection of charmed mesons misidentified as τ leptons, as originally developed for the $B^0 \to K^{*0}\tau^\pm\mu^\mp$ search [15]. The τ lepton predominantly decays into three charged pions and a neutrino through the $a_1^\pm$ resonance, which in turn decays into ρ^0 and $\pi^\pm$ mesons. In order to exploit the kinematic properties of this decay chain, the multivariate selection uses the minimum and maximum of the momenta of the pions from the τ candidate and the masses of pion

JHEP11(2025)172

pairs with zero combined charge. The threshold optimisation follows the same approach used for the first multivariate selection.

The fourth selection step consists of particle-identification (PID) requirements on the final-state particles. Three PID variables, each related to the final-state particle species (electron, kaon and pion) are used. A three-dimensional scan over the possible thresholds of the three particle-identification criteria is performed and a configuration maximising the Punzi figure of merit is chosen. For this optimisation, the background yields evaluated in the previous step are multiplied by the rejection of the particle-identification requirements, as estimated from same-sign events within the signal region.

Further background is removed by exploiting the discriminating power of the K^{*0} candidates' invariant mass, required to be within $842 < m(K^{*0}) < 970\,\text{MeV}/c^2$ as a result of an optimisation using the Punzi figure of merit.

Additionally, selection criteria are imposed on the logarithms of the tau flight distance from the B^0 vertex and its significance to eliminate residual physics backgrounds. These requirements have no impact on the events in the selected sidebands, but they reduce additional background components that are present in the control regions used for the background parameterisation.

The remaining physics backgrounds are studied with candidates rejected by the first multivariate selection within the signal region. Mass distributions from all possible final-state particle combinations, including particle misidentification, are analysed, and vetoes are imposed to remove the observed resonant structures. For example, $B^0 \to D^{*-}e^+\nu_e$ decays, with $D^{*-} \to \overline{D}{}^0\pi^-$ and $\overline{D}{}^0 \to K^+\pi^-\pi^+\pi^-$ decays and analogous contributions from the $D_0^*(2300)$ and $D_2^*(2460)$ resonances, are a background for the $B^0 \to K^{*0}\tau^-e^+$ mode if three of the four pions are misreconstructed as a τ candidate and the remaining pion and kaon mimic a K^{*0} candidate. A similar background comes from $B^0 \to D_1(2420)^-e^+\nu_e$ decays with $D_1(2420)^- \to D^-\pi^+\pi^-$ and $D^- \to K^+\pi^-\pi^-$. These two categories of decays are background also for the $B^0 \to K^{*0}\tau^+e^-$ mode, though, for charge conservation, this additionally requires misidentification of both a pion and an electron. To reduce these backgrounds from charmed mesons, candidates with $m(K^+\tau^-)$ or $m(K^{*0}\pi^-\pi^+)$ within $\pm 60\,\text{MeV}/c^2$ of the known D^0 mass [48] and candidates with $m(K^{*0}\pi^-)$ or $m(K^+\pi^-\pi^-)$ within $\pm 60\,\text{MeV}/c^2$ of the known D^- mass [48] are removed. Additionally, for the $B^0 \to K^{*0}\tau^+e^-$ mode, candidates are excluded if the invariant mass of $K^{*0}e^-$ or $K^+\pi^-e^-$ combinations, calculated by assigning the pion mass to the electron, lies within $\pm 60\,\text{MeV}/c^2$ of the known D^- mass [48]. No other significant contributions from decays with charmed mesons are observed. For the $B^0 \to K^{*0}\tau^+e^-$ mode, $B^0 \to D^{*-}\tau^+\nu_\tau$ decays with $D^{*-} \to \overline{D}{}^0\pi^-$, $\overline{D}{}^0 \to K^+e^-\overline{\nu}_e$ and $\tau^+ \to \pi^+\pi^-\pi^+\overline{\nu}_\tau$ decays constitute an irreducible background. This background does not peak in the invariant-mass distribution of the kaon and electron due to the missing energy carried by neutrinos. Thus, its contribution is assumed to be absorbed in the background shape parameterisation used in the fit.

After the selection procedure described above, there is never more than one B^0 candidate selected per event.

JHEP11(2025)172

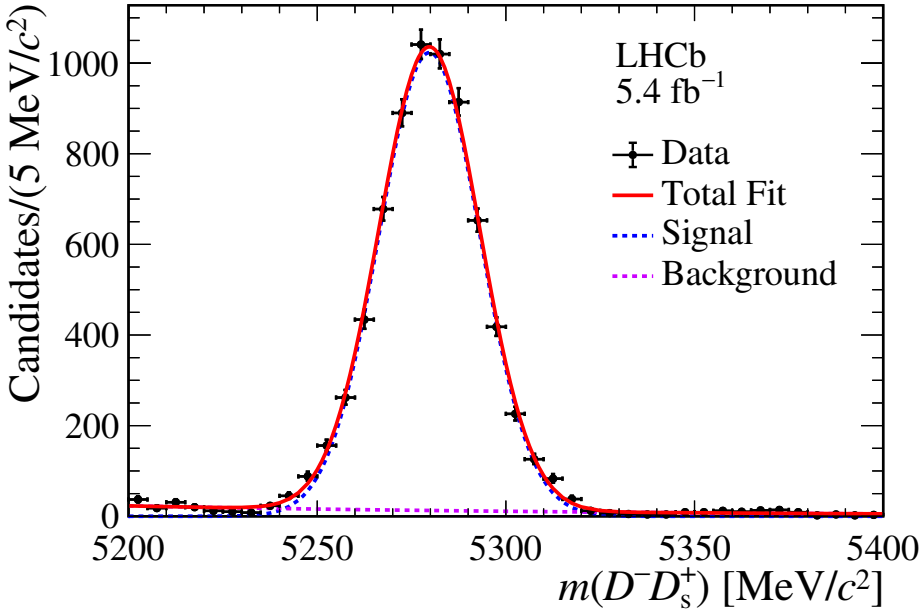

Figure 2. Invariant-mass distribution of selected $D^-D_s^+$ candidates along with the fit result.

5 Normalisation channel

The normalisation channel $B^0 \to D^-D_s^+$, with $D^- \to K^+\pi^-\pi^-$ and $D_s^+ \to K^+K^-\pi^+$ decays, is reconstructed using six tracks, each with momentum $2 < p < 110\,\text{GeV}/c$, $p_\text{T} > 250\,\text{MeV}/c$, pseudorapidity in range $2.0 < \eta < 4.9$ and PID information from the RICH detectors. Three of these tracks, one identified as a kaon and the other two as pions, originating from a common vertex, displaced from the PV, are used to form a D^- candidate. An invariant mass within $\pm 40\,\text{MeV}/c^2$ of the known D^- mass [48] is also required. Analogously, one track that is identified as a pion, and two tracks identified as kaons, are used to form a D_s^+ candidate with a displaced vertex and an invariant mass within $\pm 40\,\text{MeV}/c^2$ of the known D_s^+ mass [48]. The same particle-identification requirements used for selecting the signal are applied to the kaon and pion candidates.

The normalisation channel yields are measured from unbinned maximum-likelihood fits of the B^0-candidate invariant-mass distribution in the range $5200 < m(D^-D_s^+) < 5400\,\text{MeV}/c^2$, separately for each year of data taking. The fit model consists of a Gaussian function to parameterise the signal component and an exponential function to describe the background. The fits lead to yields of $2\,054 \pm 45$, $2\,086 \pm 45$ and $2\,730 \pm 52$ events for the 2016, 2017 and 2018 datasets, respectively. The mass distribution of the normalisation candidates for the combined dataset, along with the fit results, is shown in figure 2.

6 Determination of efficiencies

The efficiencies for the different steps of the selection chain are evaluated separately for each year of data taking and for the $B^0 \to K^{*0}\tau^+e^-$ and $B^0 \to K^{*0}\tau^-e^+$ decay channels. With the exception of the particle-identification efficiency and the normalisation-channel hardware

JHEP11(2025)172

trigger efficiency, which are directly estimated from data, all efficiencies are estimated from simulation. Electron reconstruction and hardware trigger efficiencies, after being estimated with simulation, are corrected via calibration samples. The reliability of the simulation is assessed using B^0, D^- and D_s^+ candidates from the normalisation channel $B^0 \to D^- D_s^+$ as proxies for two- and three-prong particle vertices, selected with the additional requirement that the B^0-candidate mass lies within $\pm 50\,\mathrm{MeV}/c^2$ of its known value [48]. All the variables used in the multivariate selections are reasonably well described by simulation, with the impact of residual discrepancies assessed as a systematic uncertainty.

The corrections to the electron reconstruction efficiencies are evaluated by comparing the reconstruction efficiencies from simulation and data in $B^+ \to J/\psi\ (\to e^+e^-)K^+$ decays, estimated using the "tag and probe" method as documented in ref. [55]. The corrections are evaluated per year of data taking as a function of the electron p_{T}, η and ϕ. They are estimated between 1 and 2%.

Hardware trigger efficiencies are calibrated by comparing the reconstruction efficiencies from simulation and data in $B^+ \to J/\psi\ (\to e^+e^-)K^+$ decays for the eTOS category and $B^0 \to D^- D_s^+$ decays for the TIS and hTOS categories [56]. Corrections are estimated as a function of relevant variables related to the particle that triggered the event: electron E_{T} and electromagnetic-calorimeter granularity for eTOS; hadron E_{T} and hadronic-calorimeter granularity for hTOS; p_{T} of the B^0 meson for TIS, which accounts for the correlation with the other b hadron in the event. These corrections lead to variations of up to $\sim 15\%$ on the hardware trigger efficiencies estimated from simulation. For the normalisation channel, the efficiency of the hardware hadron trigger is evaluated directly from data as the fraction of events triggered by both any muon and one of the hadrons from the $B^0 \to D^- D_s^+$ decay, relative to those triggered by any muon alone.

The particle-identification efficiency is evaluated using data calibration samples, separately for each year of data taking. A pure sample of pions and kaons is obtained from the decay $D^{*+} \to D^0(\to K\pi)\pi^+$, while a pure sample of electrons is obtained from $B^+ \to J/\psi(\to e^+e^-)K^+$ decays, without relying on PID selection criteria [57]. The efficiency of the PID requirements is then computed in intervals of the kinematic variables of the final-state particle momentum and pseudorapidity [58]. Intervals are chosen to balance the stability of the efficiency within each interval and the statistical uncertainty. The event occupancy, parameterised by the number of tracks per event, is also considered, relying on observed distributions from same-sign events in the case of signal, and the data distribution itself for the normalisation channel.

The reconstruction and selection efficiency is determined from simulation, assuming a phase-space model for signal, i.e., a uniform distribution of candidates as a function of the angular observables. The efficiency is not uniform as function of the relevant kinematic observables, which are the four-momentum-transfer q^2 and the three angular observables φ, $\cos(\vartheta_l)$ and $\cos(\vartheta_K)$, defined as in ref. [59]. The distributions of the efficiency as a function of these variables are provided in appendix A. These distributions can be used to interpret the results for models having $B^0 \to K^{*0}\tau^- e^+$ and $B^0 \to K^{*0}\tau^+ e^-$ decay kinematics different from the phase-space model used in this search.

JHEP11(2025)172

7 Fit strategy

An extended unbinned maximum-likelihood fit is performed independently on the $m_{\rm fit}$ distributions for the $B^0 \to K^{*0}\tau^+e^-$ and $B^0 \to K^{*0}\tau^-e^+$ decay channels. For each channel the distribution is described by a function $P_{\rm tot}$, which is the sum of three components, $P_{\rm tot} = Y_{3\pi}P_{3\pi} + Y_{3\pi\pi^0}P_{3\pi\pi^0} + Y_{\rm bkg}P_{\rm bkg}$. The function $P_{3\pi}$ models the dominant signal contribution with $\tau^- \to \pi^-\pi^+\pi^-\nu_\tau$ and $Y_{3\pi}$ indicates the corresponding yield. Analogously, $P_{3\pi\pi^0}$ models the subdominant signal contribution with $\tau^- \to \pi^-\pi^+\pi^-\pi^0\nu_\tau$ and $Y_{3\pi\pi^0}$ represents the corresponding yield. Finally, $P_{\rm bkg}$ models the background, with yield parameter $Y_{\rm bkg}$.

The signal components $P_{3\pi}$ and $P_{3\pi\pi^0}$ are parameterised independently, as they are expected to have slightly different shapes. For each of the components, the sum of two double-sided Crystal Ball functions (DSCB) are used, accounting for candidates with and without bremsstrahlung recovery. The fraction of candidates with bremsstrahlung recovery is fixed from simulation. A DSCB is a Crystal Ball function [60] with an additional power-law tail on the right side of the peak. The parameters are determined and fixed from fits to the simulated signal samples. The yields for the dominant signal contribution are expressed for the $B^0 \to K^{*0}\tau^+e^-$ channel as

$$Y_{3\pi} = \frac{\mathcal{B}(B^0 \to K^{*0}\tau^+e^-)\mathcal{B}(K^{*0} \to K^+\pi^-)\mathcal{B}(\tau^- \to \pi^-\pi^+\pi^-\nu_\tau)}{\mathcal{B}(B^0 \to D^-D_s^+)\mathcal{B}(D^- \to K^+\pi^-\pi^-)\mathcal{B}(D_s^+ \to K^+K^-\pi^+)} \sum_{i\in\text{year}} \left(\frac{\varepsilon Y_{\rm N}}{\varepsilon_{\rm N}}\right)_i. \tag{7.1}$$

Analogous expressions hold for the $B^0 \to K^{*0}\tau^-e^+$ channel and for the subdominant signal components. Here, ε represents the signal efficiency, while $Y_{\rm N}$ and $\varepsilon_{\rm N}$ indicate the yield and efficiency for the normalisation channel. The ratio $\varepsilon Y_{\rm N}/\varepsilon_{\rm N}$ is calculated for each year, as indicated by the i index. The branching fractions are taken from ref. [48], with the exception of the parameter of interest $\mathcal{B}(B^0 \to K^{*0}\tau^+e^-)$, common among the yields of the dominant and subdominant signal contributions, and determined from the simultaneous fit. A bias on the measured signal branching ratio, at the level of 10^{-7}, is evaluated with background-only pseudoexperiments and subtracted. All other parameters are constrained with Gaussian functions to account for the systematic uncertainties described in the next section.

An empirical functional form is used to parametrise the background shape. Based on a control sample obtained by inverting the combinatorial multivariate selection on the selected $B^0 \to K^{*0}\tau^+e^-$ and $B^0 \to K^{*0}\tau^-e^+$ candidates, a DSCB function is chosen. The shape parameters are constrained to the values determined from the control sample fit, while the background yields are allowed to vary freely. Signal contamination in the control sample is estimated to be less than 5% of the total signal, assuming a branching fraction of 10^{-5}.

8 Systematic uncertainties

In the ratios of signal and normalisation-channel efficiencies, systematic uncertainties largely cancel. The uncertainty related to the limited size of the simulation samples used to determine the efficiencies is included. Residual systematic effects in the ratio are assessed as described in the following.

The conversion of the signal yields into their respective branching fractions involves external input from known intermediate branching fractions. The corresponding systematic uncertainty is assigned by imposing constraints using Gaussian priors from ref. [48].

JHEP11(2025)172

The systematic uncertainty associated with the fit model used to measure the normalisation channel yields Y_n is assessed using pseudoexperiments generated from a kernel-density estimation of the $B^0 \to D^- D_s^+$ mass distribution and an exponential function for the background. The pseudoexperiments are subsequently fitted using the baseline model for the normalisation channel. The relative systematic uncertainty is 0.2%, evaluated as the ratio between the mean fitted and generated yields.

The ratio of the tracking efficiency between the signal and normalisation channels is determined from simulation. Possible differences between data and simulation largely cancel in the ratio. Since the sixth hadron in the normalisation channel interacts differently with the material with respect to the electron in the signal channel, in the tracking efficiency ratios, a 1.4% uncertainty is assigned to the hadron [61] and a 0.6% uncertainty to the electron [55], evaluated with data control samples.

The systematic uncertainty in determining the efficiency of the PID selection considers the limited size of the simulation and calibration samples; choice of the bin size of p, η and the number of tracks; and the use of the sPlot technique [62] to extract the signal yield in the control samples.

Although the simulation of the variables used in the multivariate classifiers is validated with the normalisation channel, small residual discrepancies could affect the evaluation of the classifier efficiencies. To account for this, the background is statistically subtracted from the $B^0 \to D^- D_s^+$ sample candidates by fitting their mass distribution after the selection, as previously described (see figure 2). The variables of the classifiers relative to the τ lepton are applied to the D^- meson and those of the K^{*0} meson are applied to the D_s^+ meson. For each classifier, the requirement giving an efficiency on the $B^0 \to D^- D_s^+$ simulation sample equivalent to that obtained by the requirement on the simulated $B^0 \to K^{*0}\tau^{\mp}e^{\pm}$ sample is applied. The relative systematic uncertainty is defined as the absolute difference in the efficiencies of this requirement between the $B^0 \to D^- D_s^+$ simulation and data, divided by the efficiency in simulation.

The calibration procedure of the hardware trigger efficiency, performed separately for each trigger category, has associated systematic effects. The first uncertainty is related to the limited size of the data and simulation samples used. In addition, the impact of different binning schemes is checked for the relevant variables used by the calibration. This turns out to be the dominant systematic effect for the hardware trigger efficiencies. For the TIS category, the p_{T} distribution of the B meson, taken by default from simulation, is also corrected using the $B^0 \to D^- D_s^+$ data sample to assess the impact on the determination of the TIS efficiency. The largest difference in the efficiency obtained using data samples alternative to that used in the baseline is also accounted for as an uncertainty. Conversely, for the software trigger, no significant discrepancy is observed between the efficiencies determined from simulation and from the high purity $B^0 \to D^- D_s^+$ sample.

Another source of systematic uncertainty is connected to the description of the background model. The parameters of the DSCB function describing the background are constrained using Gaussian priors derived from a fit to a background control region, obtained by loosening the combinatorial multivariate selection. Alternative control regions are defined by choosing different requirements on the combinatorial multivariate discriminant, Fisher discriminant

JHEP11(2025)172

Systematic effect	Upper limit increase [%]	
	$B^0 \to K^{*0}\tau^+e^-$	$B^0 \to K^{*0}\tau^-e^+$
Input branching fractions	2.3	2.5
Normalisation yields	<0.1	<0.1
Efficiencies	1.2	1.0
Background model	4.7	5.2
Signal model	1.2	0.5
Total	9.7	9.5

Table 1. Relative increase of the observed upper limit when applying each systematic uncertainty in turn. Each number is expressed as a function of the previous step, while the total is relative to the case when no systematic is included.

and the K^{*0} mass window, one by one. The peak position and width of the DSCB function are Gaussian-constrained with a width of $\sim 2\%$ and $\sim 14\%$ respectively, accounting for their variation in these alternative control regions.

In addition, a systematic uncertainty is assigned to the choice of the DSCB functional form. This is assessed by generating samples via a kernel-density estimation of background control samples and fitting them with the DSCB function. This systematic is added to each of the signal branching fractions, constraining its value with a Gaussian function with a mean of zero and a width set to the average value of the bias measured on the pseudoexperiments, which is at the level of 10^{-7}. The systematic uncertainty on the signal model includes a contribution associated with the reliability of the mass reconstruction technique. It is assessed by reconstructing $B^0 \to D^- D_s^+$ candidates with only five tracks, thus emulating the missing energy carried by the neutrino from the τ decay in the signal channel. The $m_{\rm fit}$ distribution is then fit in the region $5150 < m_{\rm fit} < 5420$ MeV/c^2, both for selected simulated and data candidates, parameterising the signal with a DSCB function with symmetric widths and the background with an exponential function. Discrepancies between data and simulation on the peak position and the widths of the DSCB are summed in quadrature, with the statistical uncertainties coming from the determination of their values from simulation. The results are used to constrain using Gaussian prior the fit to the data. Additionally, the signal-model systematic uncertainty has a component related to the fraction of bremsstrahlung candidates taken from the simulation. The statistical uncertainty of the simulation sample is combined with the largest discrepancy between the fraction of bremsstrahlung candidates in data and simulation evaluated in $B^0 \to K^{*0} J/\psi(\to e^+e^-)$ decays, as described in ref. [63].

The increase of the observed upper limit when progressively adding each of the systematic uncertainties is shown in table 1. The dominant systematic effect comes from the uncertainty on the arbitrary choice of the background control region.

JHEP11(2025)172

Model	Upper limit $[10^{-6}]$	
	$B^0 \to K^{*0}\tau^- e^+$	$B^0 \to K^{*0}\tau^+ e^-$
Phase space (PHSP)	5.9 (7.1)	4.9 (5.9)
Left-handed ($C_9^{\tau e} = -C_{10}^{\tau e} \neq 0$)	6.3 (7.7)	5.4 (6.4)
Scalar ($C_S^{\tau e} \neq 0$)	6.6 (8.0)	5.7 (6.8)

Table 2. Upper limits on the branching fraction of the decays for the assumed phase-space model and two beyond the SM scenarios, at 90% (95%) confidence level.

9 Results

The results of the extended unbinned maximum-likelihood fit to the m_{fit} distributions are shown in figure 3, with the corresponding likelihood-ratio scans, with all nuisance parameters profiled, shown in figure 4. The likelihood ratio is defined as the likelihood of the hypothesis with no signal over the likelihood of the hypothesis of a nonzero branching fraction. No significant signal contribution is observed and the measured branching fractions correspond to $\mathcal{B}(B^0 \to K^{*0}\tau^- e^+) = (1.7 \pm 2.5) \times 10^{-6}$ and $\mathcal{B}(B^0 \to K^{*0}\tau^+ e^-) = (1.8 \pm 1.9) \times 10^{-6}$, accounting for both statistical and systematic sources of uncertainties. Therefore, upper limits on the branching fractions are set using the CL_s method with the asymptotic approximation [64, 65]:

$$\mathcal{B}(B^0 \to K^{*0}\tau^- e^+) < 5.9\ (7.1) \times 10^{-6}$$

and

$$\mathcal{B}(B^0 \to K^{*0}\tau^+ e^-) < 4.9\ (5.9) \times 10^{-6}$$

at the 90% (95)% confidence level, as shown in figure 5.

These results are obtained assuming a phase-space model for the signal decays. When computing limits in alternative scenarios, the variation of the reconstruction and selection efficiency with decay kinematics given in appendix A needs to be accounted for.

As an example, two scenarios of physics beyond the SM are considered in this study: a left-handed model with $C_9^{\tau e} = -C_{10}^{\tau e} \neq 0$ and a scalar model with $C_S^{\tau e} \neq 0$, where $C_i^{\tau e}$ are the lepton-flavour-violating Wilson coefficients [66]. For these scenarios, the comparison with phase-space kinematics is shown in appendix B. The resulting limits are presented in table 2.

JHEP11(2025)172

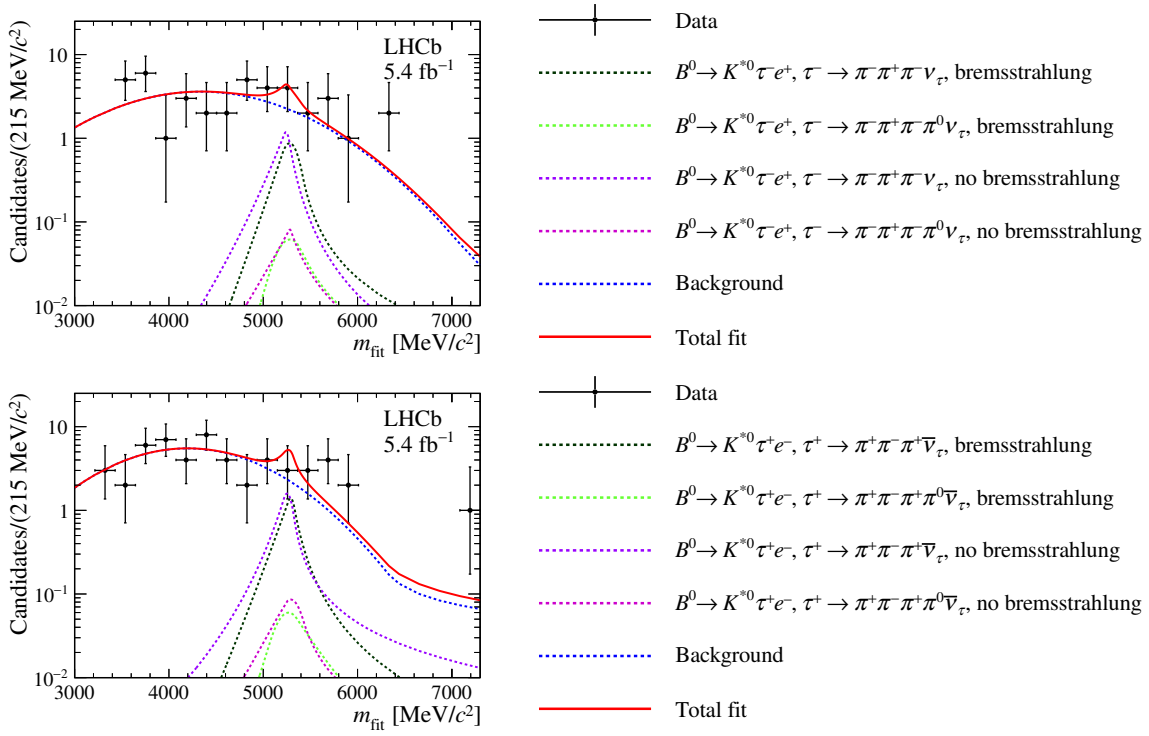

Figure 3. Distribution of the mass $m_{\rm fit}$ of (top) $B^0\to K^{*0}\tau^-e^+$ and (bottom) $B^0\to K^{*0}\tau^+e^-$ selected candidates, with the simultaneous fit result. Legends with the various components of the fit are shown next to the plots.

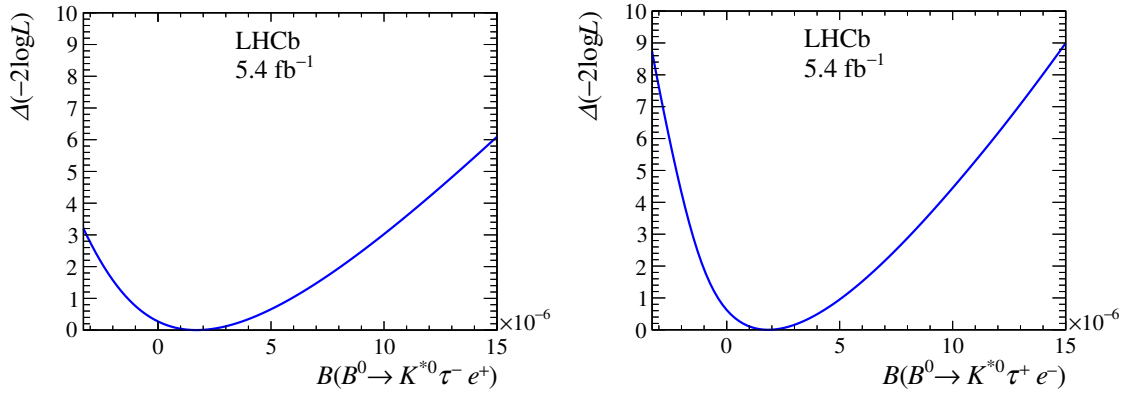

Figure 4. Likelihood-ratio scans for the (left) $B^0\to K^{*0}\tau^-e^+$ and (right) $B^0\to K^{*0}\tau^+e^-$ branching fraction with all nuisance parameters profiled.

JHEP11(2025)172

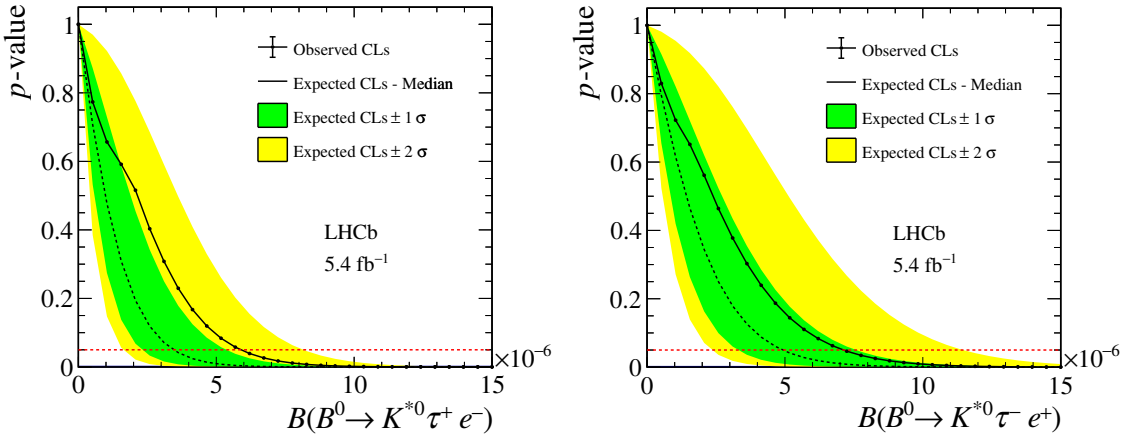

Figure 5. The expected and observed p-values derived with the CL_s method as a function of the (left) $B^0 \to K^{*0}\tau^- e^+$ and (right) $B^0 \to K^{*0}\tau^+ e^-$ branching fraction. The red line corresponds to the 95% CL.

10 Conclusion

This study presents the first search at LHCb for the lepton-flavour-violating decays $B^0 \to K^{*0}\tau^\pm e^\mp$, performed on a sample of proton-proton collision data collected with the LHCb detector at a centre-of-mass energy of 13 TeV between 2016 and 2018, and corresponding to an integrated luminosity of 5.4 fb^{-1}. No significant signal is observed, and upper limits on the branching fractions are set: $\mathcal{B}(B^0 \to K^{*0}\tau^- e^+) < 5.9\ (7.1) \times 10^{-6}$ and $\mathcal{B}(B^0 \to K^{*0}\tau^+ e^-) < 4.9\ (5.9) \times 10^{-6}$ at the 90% (95%) confidence level. These results assume a uniform distribution of the signal events within the phase space accessible to the K^{*0}, τ, and electron, and are the most stringent upper limits to date on $b \to s\tau e$ transitions.

Acknowledgments

We express our gratitude to our colleagues in the CERN accelerator departments for the excellent performance of the LHC. We thank the technical and administrative staff at the LHCb institutes. We acknowledge support from CERN and from the national agencies: ARC (Australia); CAPES, CNPq, FAPERJ and FINEP (Brazil); MOST and NSFC (China); CNRS/IN2P3 (France); BMFTR, DFG and MPG (Germany); INFN (Italy); NWO (Netherlands); MNiSW and NCN (Poland); MCID/IFA (Romania); MICIU and AEI (Spain); SNSF and SER (Switzerland); NASU (Ukraine); STFC (United Kingdom); DOE NP and NSF (U.S.A.). We acknowledge the computing resources that are provided by ARDC (Australia), CBPF (Brazil), CERN, IHEP and LZU (China), IN2P3 (France), KIT and DESY (Germany), INFN (Italy), SURF (Netherlands), Polish WLCG (Poland), IFIN-HH (Romania), PIC (Spain), CSCS (Switzerland), and GridPP (United Kingdom). We are indebted to the communities behind the multiple open-source software packages on which we depend. Individual groups or members have received support from Key Research Program of Frontier Sciences of CAS, CAS PIFI, CAS CCEPP, Fundamental Research Funds for the Central Universities, and Sci. & Tech. Program of Guangzhou (China); Minciencias (Colombia); EPLANET, Marie

JHEP11(2025)172

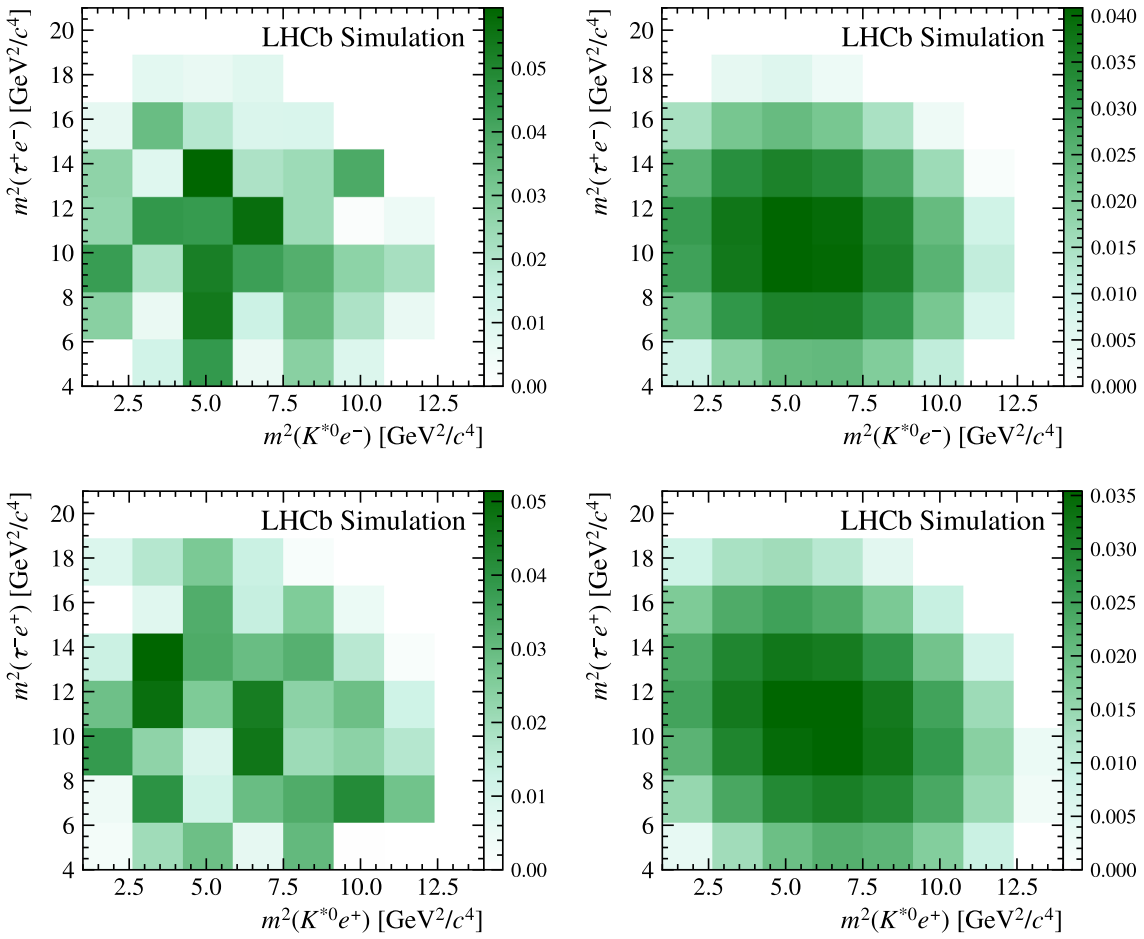

Figure 6. Efficiency distribution as a function of (left) $m^2_{K^{*0}e^\pm}$ and $m^2_{\tau^\mp e^\pm}$ with (right) their bidimensional polynomial fits for (top) the $B^0 \to K^{*0}\tau^+e^-$ and (bottom) $B^0 \to K^{*0}\tau^-e^+$ cases, normalised to unity.

Skłodowska-Curie Actions, ERC and NextGenerationEU (European Union); A*MIDEX, ANR, IPhU and Labex P2IO, and Région Auvergne-Rhône-Alpes (France); Alexander-von-Humboldt Foundation (Germany); ICSC (Italy); Severo Ochoa and María de Maeztu Units of Excellence, GVA, XuntaGal, GENCAT, InTalent-Inditex and Prog. Atracción Talento CM (Spain); SRC (Sweden); the Leverhulme Trust, the Royal Society and UKRI (United Kingdom).

A Efficiencies as function of kinematics

Efficiency as function of the four-momentum transfer $q^2 = m^2(\tau^\pm e^\mp)$ and $m^2(K^{*0}\tau^\pm)$ (figure 6) and as function of q^2 and the three decay angles φ, $\cos(\vartheta_l)$ and $\cos(\vartheta_K)$ (figures 7, 8, 9, 10), defined as in ref. [59], are presented.

JHEP11(2025)172

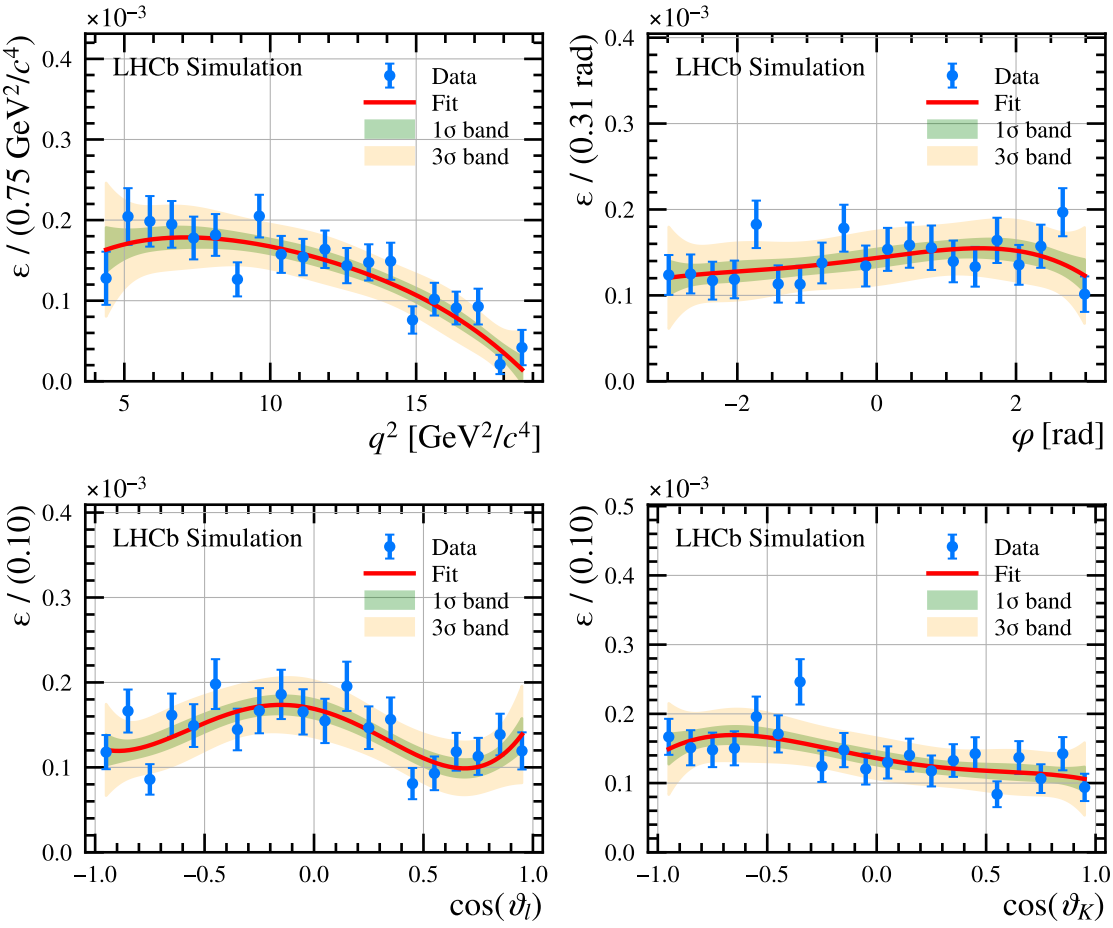

Figure 7. Efficiency distributions with their polynomial fit results as a function of (top left) q^2, (top right) φ, (bottom left) $\cos(\vartheta_l)$ and (bottom right) $\cos(\vartheta_K)$ for $B^0 \to K^{*0}\tau^+e^-$ and $\tau^+ \to \pi^+\pi^-\pi^+\bar{\nu_\tau}$ decays.

JHEP11(2025)172

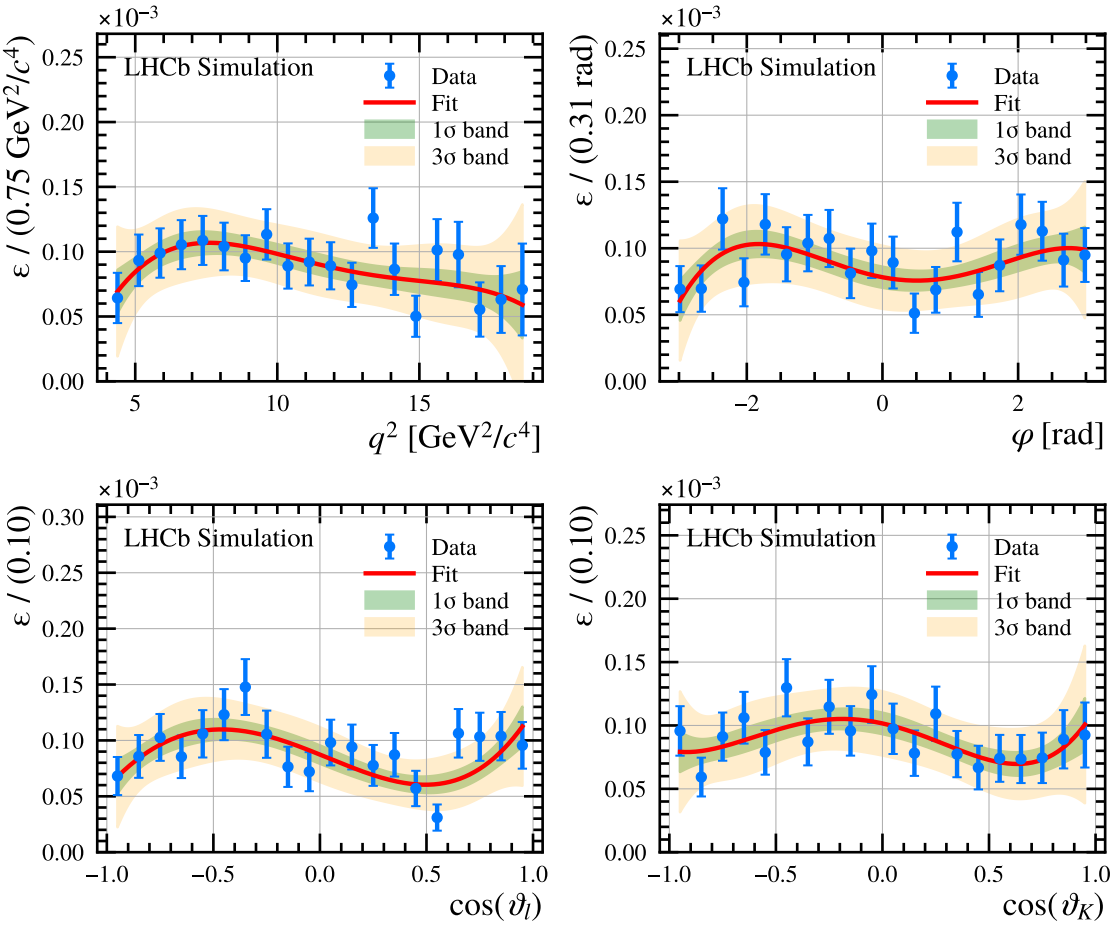

Figure 8. Efficiency distributions with their polynomial fit results as a function of (top left) q^2, (top right) φ, (bottom left) $\cos(\vartheta_l)$ and (bottom right) $\cos(\vartheta_K)$ for $B^0 \to K^{*0}\tau^+e^-$ and $\tau^+ \to \pi^+\pi^-\pi^+\pi^0\bar{\nu_\tau}$ decays.

JHEP11(2025)172

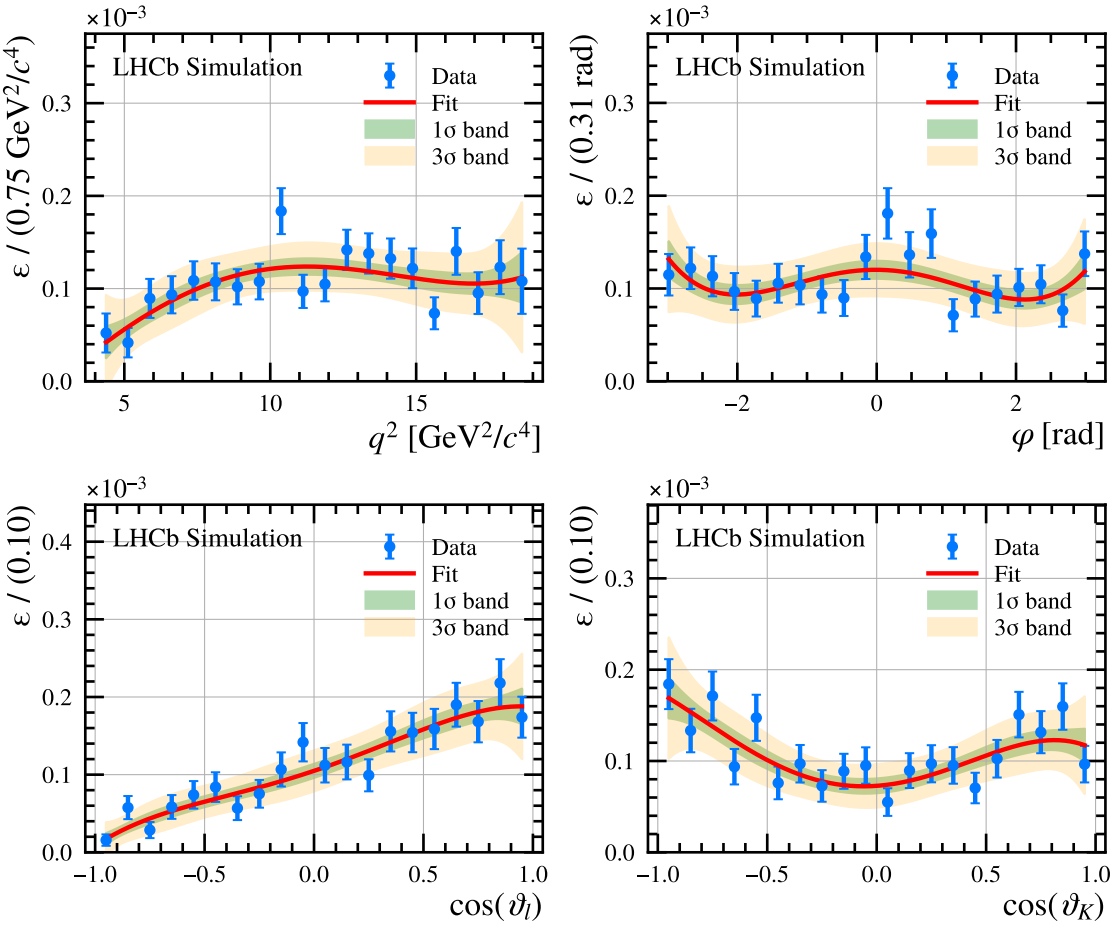

Figure 9. Efficiency distributions with their polynomial fit results as a function of (top left) q^2, (top right) φ, (bottom left) $\cos(\vartheta_l)$ and (bottom right) $\cos(\vartheta_K)$ for $B^0 \to K^{*0}\tau^- e^+$ and $\tau^- \to \pi^-\pi^+\pi^-\nu_\tau$ decays.

JHEP11(2025)172

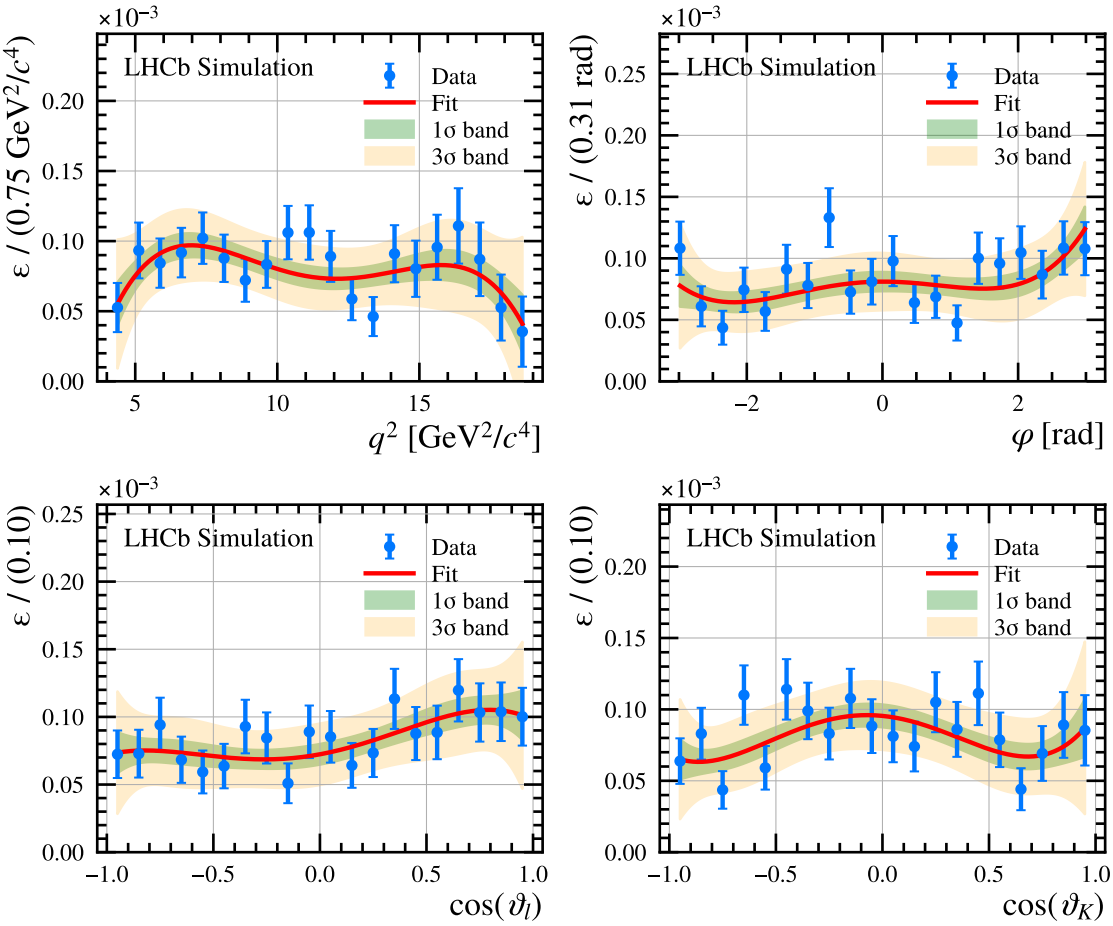

Figure 10. Efficiency distributions with their polynomial fit results as a function of (top left) q^2, (top right) φ, (bottom left) $\cos(\vartheta_l)$ and (bottom right) $\cos(\vartheta_K)$ for $B^0 \to K^{*0}\tau^-e^+$ and $\tau^- \to \pi^-\pi^+\pi^-\pi^0\nu_\tau$ decays.

JHEP11(2025)172

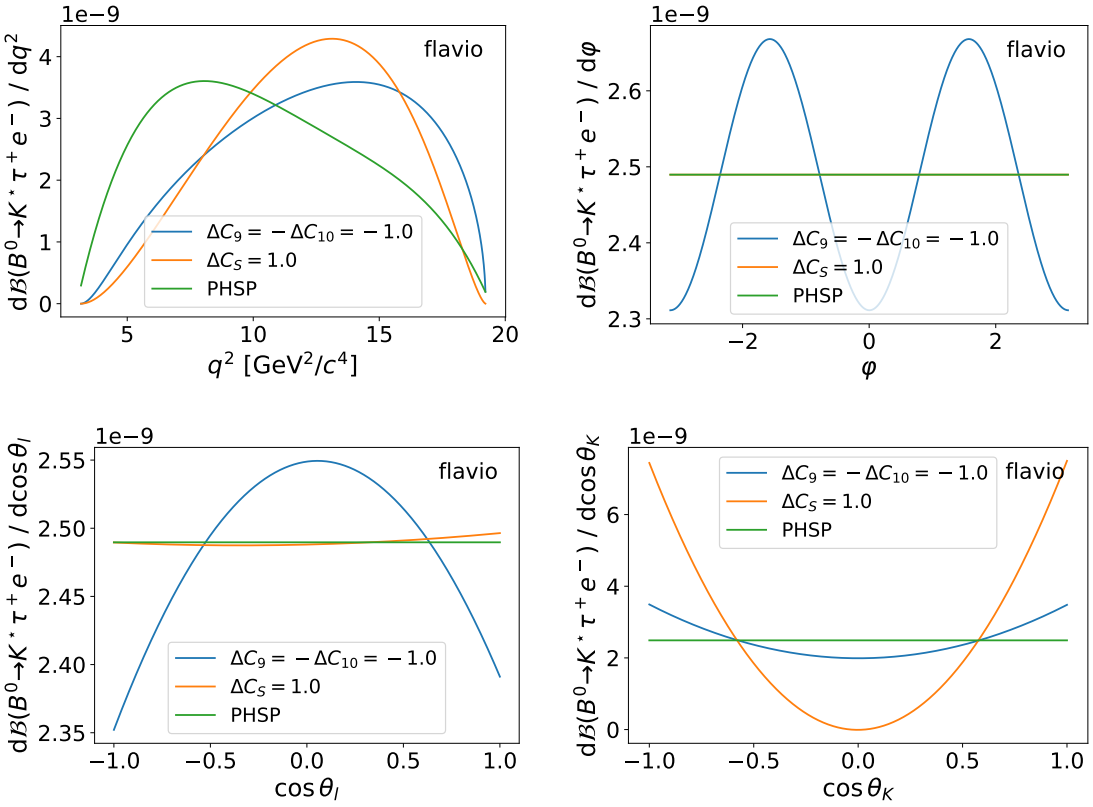

Figure 11. Differential decay rates as function of kinematics in different models for $B^0 \to K^{*0}\tau^+e^-$ decays. Distributions are normalised to the integrated branching ratio obtained with the left-handed model ($\Delta C_9^{e\tau} = -\Delta C_{10}^{e\tau} = -1$).

B Beyond the Standard Model scenarios

Scenarios beyond the Standard Model can result in very different distributions in four-momentum transfer $q^2 = m^2(\tau^\pm e^\mp)$ and the three decay angles φ, $\cos(\vartheta_l)$ and $\cos(\vartheta_K)$, defined as in ref. [59]. This is illustrated in figures 11 and 12, obtained using the python package FLAVIO [67].

JHEP11(2025)172

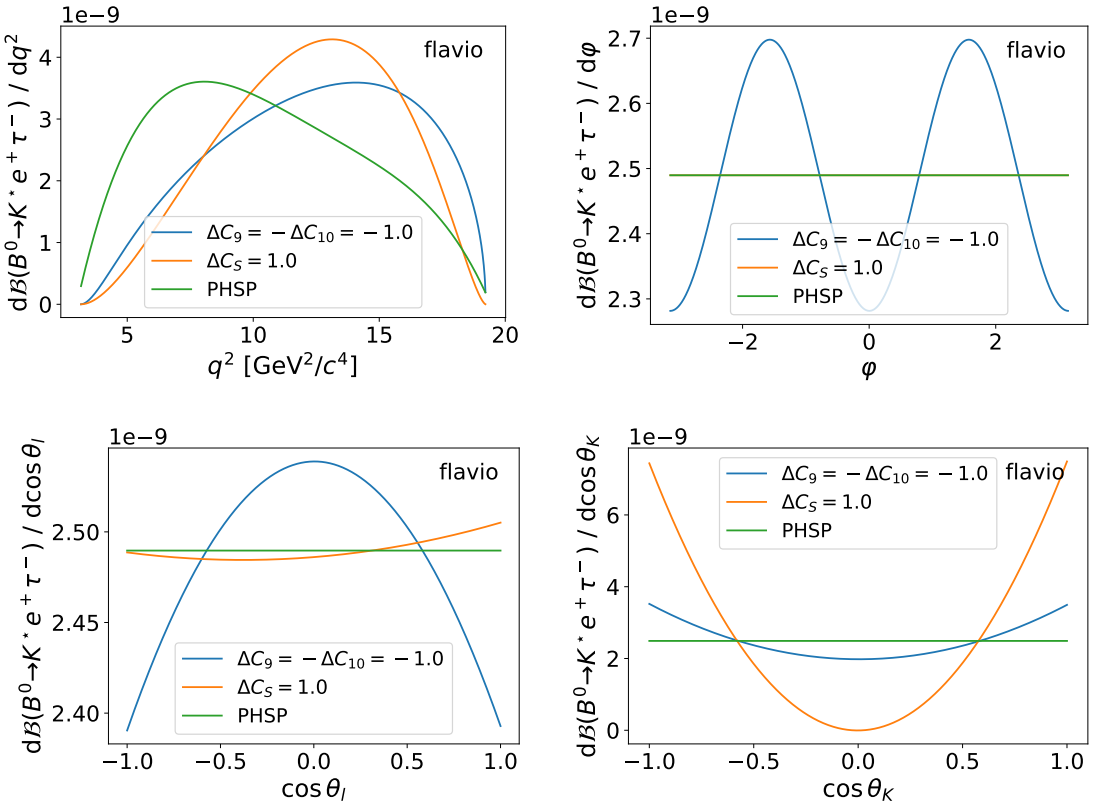

Figure 12. Differential decay rates as function of kinematics in different models for $B^0 \to K^{*0}\tau^- e^+$ decays. Distributions are normalised to the integrated branching ratio obtained with the left-handed model ($\Delta C_9^{e\tau} = -\Delta C_{10}^{e\tau} = -1$).

JHEP11(2025)172

Data Availability Statement. Data associated to the plots in this publication are made available on the CERN Document Server in ref. [68].

Code Availability Statement. This article has no associated code or the code will not be deposited.

References

[1] Super-Kamiokande collaboration, *Evidence for oscillation of atmospheric neutrinos*, *Phys. Rev. Lett.* **81** (1998) 1562 [hep-ex/9807003] [INSPIRE].

[2] SNO collaboration, *Measurement of the rate of $\nu_e + d \to p + p + e^-$ interactions produced by ^8B solar neutrinos at the Sudbury Neutrino Observatory*, *Phys. Rev. Lett.* **87** (2001) 071301 [nucl-ex/0106015] [INSPIRE].

[3] OPERA collaboration, *Observation of a first ν_τ candidate in the OPERA experiment in the CNGS beam*, *Phys. Lett. B* **691** (2010) 138 [arXiv:1006.1623] [INSPIRE].

[4] T2K collaboration, *Evidence of electron neutrino appearance in a muon neutrino beam*, *Phys. Rev. D* **88** (2013) 032002 [arXiv:1304.0841] [INSPIRE].

[5] NOvA collaboration, *First measurement of muon-neutrino disappearance in NOvA*, *Phys. Rev. D* **93** (2016) 051104 [arXiv:1601.05037] [INSPIRE].

[6] Double Chooz collaboration, *Indication of reactor $\bar{\nu}_e$ disappearance in the double Chooz experiment*, *Phys. Rev. Lett.* **108** (2012) 131801 [arXiv:1112.6353] [INSPIRE].

[7] Daya Bay collaboration, *Observation of electron-antineutrino disappearance at Daya Bay*, *Phys. Rev. Lett.* **108** (2012) 171803 [arXiv:1203.1669] [INSPIRE].

[8] RENO collaboration, *Observation of reactor electron antineutrino disappearance in the RENO experiment*, *Phys. Rev. Lett.* **108** (2012) 191802 [arXiv:1204.0626] [INSPIRE].

[9] M. Raidal et al., *Flavour physics of leptons and dipole moments*, *Eur. Phys. J. C* **57** (2008) 13 [arXiv:0801.1826] [INSPIRE].

[10] LHCb collaboration, *Search for the lepton-flavour violating decays $B^0_{(s)} \to e^\pm \mu^\mp$*, *JHEP* **03** (2018) 078 [arXiv:1710.04111] [INSPIRE].

[11] LHCb collaboration, *Amplitude analysis of $B^\pm \to \pi^\pm K^+ K^-$ decays*, *Phys. Rev. Lett.* **123** (2019) 231802 [arXiv:1905.09244] [INSPIRE].

[12] LHCb collaboration, *Search for the lepton-flavour violating decays $B^0 \to K^{*0} \mu^\pm e^\mp$ and $B^0_s \to \phi \mu^\pm e^\mp$*, *JHEP* **06** (2023) 073 [arXiv:2207.04005] [INSPIRE].

[13] LHCb collaboration, *Search for the lepton-flavour-violating decays $B^0_s \to \tau^\pm \mu^\mp$ and $B^0 \to \tau^\pm \mu^\mp$*, *Phys. Rev. Lett.* **123** (2019) 211801 [arXiv:1905.06614] [INSPIRE].

[14] LHCb collaboration, *Search for the lepton flavour violating decay $B^+ \to K^+ \mu^- \tau^+$ using B^{*0}_{s2} decays*, *JHEP* **06** (2020) 129 [arXiv:2003.04352] [INSPIRE].

[15] LHCb collaboration, *Search for the lepton-flavour violating decays $B^0 \to K^{*0} \tau^\pm \mu^\mp$*, *JHEP* **06** (2023) 143 [arXiv:2209.09846] [INSPIRE].

JHEP11(2025)172

[16] LHCb collaboration, *Search for the lepton-flavor violating decay $B_s^0 \to \phi\mu^\pm\tau^\mp$*, *Phys. Rev. D* **110** (2024) 072014 [arXiv:2405.13103] [INSPIRE].

[17] BABAR collaboration, *Measurements of branching fractions, rate asymmetries, and angular distributions in the rare decays $B \to K\ell^+\ell^-$ and $B \to K^*\ell^+\ell^-$*, *Phys. Rev. D* **73** (2006) 092001 [hep-ex/0604007] [INSPIRE].

[18] BABAR collaboration, *Search for the rare decay $B \to \pi l^+ l^-$*, *Phys. Rev. Lett.* **99** (2007) 051801 [hep-ex/0703018] [INSPIRE].

[19] BELLE collaboration, *Search for lepton-number-violating $B^+ \to D^- l^+ l'^+$ decays*, *Phys. Rev. D* **84** (2011) 071106 [arXiv:1107.0642] [INSPIRE].

[20] BABAR collaboration, *A search for the decay modes $B^{+-} \to h^{+-}\tau^{+-}l$*, *Phys. Rev. D* **86** (2012) 012004 [arXiv:1204.2852] [INSPIRE].

[21] BABAR collaboration, *Search for lepton-number violating $B^+ \to X^-\ell^+\ell'^+$ decays*, *Phys. Rev. D* **89** (2014) 011102 [arXiv:1310.8238] [INSPIRE].

[22] BELLE collaboration, *Test of lepton flavor universality and search for lepton flavor violation in $B \to K\ell\ell$ decays*, *JHEP* **03** (2021) 105 [arXiv:1908.01848] [INSPIRE].

[23] BELLE collaboration, *Search for $B^0 \to \tau^\pm\ell^\mp$ ($\ell = e, \mu$) with a hadronic tagging method at Belle*, *Phys. Rev. D* **104** (2021) L091105 [arXiv:2108.11649] [INSPIRE].

[24] BELLE collaboration, *Search for the lepton flavor violating decays $B^+ \to K^+\tau^\pm\ell^\mp$ ($\ell = e$, μ) at Belle*, *Phys. Rev. Lett.* **130** (2023) 261802 [arXiv:2212.04128] [INSPIRE].

[25] BELLE collaboration, *Search for $B_s^0 \to \ell^\mp\tau^\pm$ with the semi-leptonic tagging method at Belle*, *JHEP* **08** (2023) 178 [arXiv:2301.10989] [INSPIRE].

[26] BELLE and BELLE-II collaborations, *Search for lepton flavor-violating decay modes $B^0 \to K^{*0}\tau^\pm\ell^\mp$ ($\ell = e, \mu$) with hadronic B-tagging at Belle and Belle II*, *JHEP* **08** (2025) 184 [arXiv:2505.08418] [INSPIRE].

[27] M. Bordone, O. Catà and T. Feldmann, *Effective theory approach to new physics with flavour: general framework and a leptoquark example*, *JHEP* **01** (2020) 067 [arXiv:1910.02641] [INSPIRE].

[28] LHCb collaboration, *The LHCb detector at the LHC*, 2008 *JINST* **3** S08005 [INSPIRE].

[29] LHCb collaboration, *LHCb detector performance*, *Int. J. Mod. Phys. A* **30** (2015) 1530022 [arXiv:1412.6352] [INSPIRE].

[30] R. Aaij et al., *Performance of the LHCb vertex locator*, 2014 *JINST* **9** P09007 [arXiv:1405.7808] [INSPIRE].

[31] LHCB OUTER TRACKER GROUP collaboration, *Performance of the LHCb outer tracker*, 2014 *JINST* **9** P01002 [arXiv:1311.3893] [INSPIRE].

[32] LHCB OUTER TRACKER GROUP collaboration, *Improved performance of the LHCb outer tracker in LHC run 2*, 2017 *JINST* **12** P11016 [arXiv:1708.00819] [INSPIRE].

[33] LHCB RICH GROUP collaboration, *Performance of the LHCb RICH detector at the LHC*, *Eur. Phys. J. C* **73** (2013) 2431 [arXiv:1211.6759] [INSPIRE].

[34] A.A. Alves Jr. et al., *Performance of the LHCb muon system*, 2013 *JINST* **8** P02022 [arXiv:1211.1346] [INSPIRE].

[35] R. Aaij et al., *The LHCb trigger and its performance in 2011*, 2013 *JINST* **8** P04022 [arXiv:1211.3055] [INSPIRE].

JHEP11(2025)172

[36] LHCb collaboration, *Design and performance of the LHCb trigger and full real-time reconstruction in run 2 of the LHC*, 2019 *JINST* **14** P04013 [arXiv:1812.10790] [INSPIRE].

[37] V.V. Gligorov and M. Williams, *Efficient, reliable and fast high-level triggering using a bonsai boosted decision tree*, 2013 *JINST* **8** P02013 [arXiv:1210.6861] [INSPIRE].

[38] T. Likhomanenko et al., *LHCb topological trigger reoptimization*, *J. Phys. Conf. Ser.* **664** (2015) 082025 [arXiv:1510.00572] [INSPIRE].

[39] T. Sjöstrand, S. Mrenna and P.Z. Skands, *A brief introduction to PYTHIA 8.1*, *Comput. Phys. Commun.* **178** (2008) 852 [arXiv:0710.3820] [INSPIRE].

[40] LHCb collaboration, *Handling of the generation of primary events in Gauss, the LHCb simulation framework*, *J. Phys. Conf. Ser.* **331** (2011) 032047 [INSPIRE].

[41] I.M. Nugent et al., *Resonance chiral Lagrangian currents and experimental data for* $\tau^- \to \pi^-\pi^-\pi^+\nu_\tau$, *Phys. Rev. D* **88** (2013) 093012 [arXiv:1310.1053] [INSPIRE].

[42] S. Jadach, Z. Was, R. Decker and J.H. Kühn, *The tau decay library TAUOLA: version 2.4*, *Comput. Phys. Commun.* **76** (1993) 361 [INSPIRE].

[43] D.J. Lange, *The EvtGen particle decay simulation package*, *Nucl. Instrum. Meth. A* **462** (2001) 152 [INSPIRE].

[44] N. Davidson, T. Przedzinski and Z. Was, *PHOTOS interface in C++: technical and physics documentation*, *Comput. Phys. Commun.* **199** (2016) 86 [arXiv:1011.0937] [INSPIRE].

[45] J. Allison et al., *GEANT4 developments and applications*, *IEEE Trans. Nucl. Sci.* **53** (2006) 270 [INSPIRE].

[46] GEANT4 collaboration, *GEANT4 — a simulation toolkit*, *Nucl. Instrum. Meth. A* **506** (2003) 250 [INSPIRE].

[47] LHCb collaboration, *The LHCb simulation application, Gauss: design, evolution and experience*, *J. Phys. Conf. Ser.* **331** (2011) 032023 [INSPIRE].

[48] Particle Data Group collaboration, *Review of particle physics*, *Phys. Rev. D* **110** (2024) 030001 [INSPIRE].

[49] W.D. Hulsbergen, *Decay chain fitting with a Kalman filter*, *Nucl. Instrum. Meth. A* **552** (2005) 566 [physics/0503191] [INSPIRE].

[50] G. Punzi, *Sensitivity of searches for new signals and its optimization*, *eConf C* **030908** (2003) MODT002 [physics/0308063] [INSPIRE].

[51] J.H. Friedman, *Greedy function approximation: a gradient boosting machine*, *Annals Statist.* **29** (2001) 1189 [INSPIRE].

[52] P. Speckmayer, A. Hocker, J. Stelzer and H. Voss, *The toolkit for multivariate data analysis, TMVA 4*, *J. Phys. Conf. Ser.* **219** (2010) 032057 [INSPIRE].

[53] A. Bevan, R.G. Goñi, T. Stevenson and T. Stevenson, *Support vector machines and generalisation in HEP*, *J. Phys. Conf. Ser.* **898** (2017) 072021 [arXiv:1702.04686] [INSPIRE].

[54] R.A. Fisher, *The use of multiple measurements in taxonomic problems*, *Annals Eugen.* **7** (1936) 179 [INSPIRE].

[55] LHCb collaboration, *Measurement of the electron reconstruction efficiency at LHCb*, 2019 *JINST* **14** P11023 [arXiv:1909.02957] [INSPIRE].

[56] S. Tolk, J. Albrecht, F. Dettori and A. Pellegrino, *Data driven trigger efficiency determination at LHCb*, LHCb-PUB-2014-039, CERN, Geneva, Switzerland (2014) [INSPIRE].

JHEP11(2025)172

[57] R. Aaij et al., *Selection and processing of calibration samples to measure the particle identification performance of the LHCb experiment in run 2*, *EPJ Tech. Instrum.* **6** (2019) 1 [arXiv:1803.00824] [INSPIRE].

[58] L. Anderlini et al., *The PIDCalib package*, LHCb-PUB-2016-021, CERN, Geneva, Switzerland (2016) [INSPIRE].

[59] LHCb collaboration, *Differential branching fraction and angular analysis of the decay* $B^0 \to K^{*0}\mu^+\mu^-$, *JHEP* **08** (2013) 131 [arXiv:1304.6325] [INSPIRE].

[60] T. Skwarnicki, *A study of the radiative CASCADE transitions between the Upsilon-Prime and Upsilon resonances*, Ph.D. thesis, INP, Cracow, Poland (1986) [INSPIRE].

[61] LHCb collaboration, *Measurement of the track reconstruction efficiency at LHCb*, 2015 *JINST* **10** P02007 [arXiv:1408.1251] [INSPIRE].

[62] M. Pivk and F.R. Le Diberder, *SPlot: a statistical tool to unfold data distributions*, *Nucl. Instrum. Meth. A* **555** (2005) 356 [physics/0402083] [INSPIRE].

[63] LHCb collaboration, *Measurement of lepton universality parameters in* $B^+ \to K^+\ell^+\ell^-$ *and* $B^0 \to K^{*0}\ell^+\ell^-$ *decays*, *Phys. Rev. D* **108** (2023) 032002 [arXiv:2212.09153] [INSPIRE].

[64] A.L. Read, *Presentation of search results: the* CL_s *technique*, *J. Phys. G* **28** (2002) 2693 [INSPIRE].

[65] G. Cowan, K. Cranmer, E. Gross and O. Vitells, *Asymptotic formulae for likelihood-based tests of new physics*, *Eur. Phys. J. C* **71** (2011) 1554 [*Erratum ibid.* **73** (2013) 2501] [arXiv:1007.1727] [INSPIRE].

[66] D. Bečirević, F. Jaffredo, J.P. Pinheiro and O. Sumensari, *Lepton flavor violation in exclusive* $b \to d\ell_i\ell_j$ *and* $b \to s\ell_i\ell_j$ *decay modes*, *Phys. Rev. D* **110** (2024) 075004 [arXiv:2407.19060] [INSPIRE].

[67] D.M. Straub, *flavio: a python package for flavour and precision phenomenology in the Standard Model and beyond*, arXiv:1810.08132 [INSPIRE].

[68] LHCb collaboration, *Search for the lepton-flavour-violating decays* $B^0 \to K^{*0}\tau^\pm e^\mp$, LHCb-PAPER-2025-005, CERN, Geneva, Switzerland (2025).

JHEP11(2025)172

The LHCb collaboration

R. Aaij[38], A.S.W. Abdelmotteleb[57], C. Abellan Beteta[51], F. Abudinén[57], T. Ackernley[61], A. A. Adefisoye[69], B. Adeva[47], M. Adinolfi[55], P. Adlarson[84], C. Agapopoulou[14], C.A. Aidala[86], Z. Ajaltouni[11], S. Akar[11], K. Akiba[38], P. Albicocco[28], J. Albrecht[19,e], F. Alessio[49], Z. Aliouche[63], P. Alvarez Cartelle[56], R. Amalric[16], S. Amato[3], J.L. Amey[55], Y. Amhis[14], L. An[6], L. Anderlini[27], M. Andersson[51], A. Andreianov[44], P. Andreola[51], M. Andreotti[26], A. Anelli[31,o,49], D. Ao[7], F. Archilli[37,v], Z Areg[69], M. Argenton[26], S. Arguedas Cuendis[9,49], A. Artamonov[44], M. Artuso[69], E. Aslanides[13], R. Ataíde Da Silva[50], M. Atzeni[65], B. Audurier[12], D. Bacher[64], I. Bachiller Perea[50], S. Bachmann[22], M. Bachmayer[50], J.J. Back[57], P. Baladron Rodriguez[47], V. Balagura[15], A. Balboni[26], W. Baldini[26], L. Balzani[19], H. Bao[7], J. Baptista de Souza Leite[61], C. Barbero Pretel[47,12], M. Barbetti[27], I. R. Barbosa[70], R.J. Barlow[63], M. Barnyakov[25], S. Barsuk[14], W. Barter[59], J. Bartz[69], S. Bashir[40], B. Batsukh[5], P. B. Battista[14], A. Bay[50], A. Beck[65], M. Becker[19], F. Bedeschi[35], I.B. Bediaga[2], N. A. Behling[19], S. Belin[47], K. Belous[44], I. Belov[29], I. Belyaev[36], G. Benane[13], G. Bencivenni[28], E. Ben-Haim[16], A. Berezhnoy[44], R. Bernet[51], S. Bernet Andres[46], A. Bertolin[33], C. Betancourt[51], F. Betti[59], J. Bex[56], Ia. Bezshyiko[51], O. Bezshyyko[85], J. Bhom[41], M.S. Bieker[18], N.V. Biesuz[26], P. Billoir[16], A. Biolchini[38], M. Birch[62], F.C.R. Bishop[10], A. Bitadze[63], A. Bizzeti[27,p], T. Blake[57], F. Blanc[50], J.E. Blank[19], S. Blusk[69], V. Bocharnikov[44], J.A. Boelhauve[19], O. Boente Garcia[15], T. Boettcher[68], A. Bohare[59], A. Boldyrev[44], C.S. Bolognani[81], R. Bolzonella[26], R. B. Bonacci[1], N. Bondar[44,49], A. Bordelius[49], F. Borgato[33,49], S. Borghi[63], M. Borsato[31,o], J.T. Borsuk[82], E. Bottalico[61], S.A. Bouchiba[50], M. Bovill[64], T.J.V. Bowcock[61], A. Boyer[49], C. Bozzi[26], J. D. Brandenburg[87], A. Brea Rodriguez[50], N. Breer[19], J. Brodzicka[41], A. Brossa Gonzalo[47,†], J. Brown[61], D. Brundu[32], E. Buchanan[59], L. Buonincontri[33,q], M. Burgos Marcos[81], A.T. Burke[63], C. Burr[49], J.S. Butter[56], J. Buytaert[49], W. Byczynski[49], S. Cadeddu[32], H. Cai[74], A. Caillet[16], R. Calabrese[26,k], S. Calderon Ramirez[9], L. Calefice[45], S. Cali[28], M. Calvi[31,o], M. Calvo Gomez[46], P. Camargo Magalhaes[2,aa], J. I. Cambon Bouzas[47], P. Campana[28], D.H. Campora Perez[81], A.F. Campoverde Quezada[7], S. Capelli[31], L. Capriotti[26], R. Caravaca-Mora[9], A. Carbone[25,i], L. Carcedo Salgado[47], R. Cardinale[29,m], A. Cardini[32], P. Carniti[31], L. Carus[22], A. Casais Vidal[65], R. Caspary[22], G. Casse[61], M. Cattaneo[49], G. Cavallero[26,49], V. Cavallini[26,k], S. Celani[22], S. Cesare[30,n], A.J. Chadwick[61], I. Chahrour[86], H. Chang[4,b], M. Charles[16], Ph. Charpentier[49], E. Chatzianagnostou[38], M. Chefdeville[10], C. Chen[56], S. Chen[5], Z. Chen[7], A. Chernov[41], S. Chernyshenko[53], X. Chiotopoulos[81], V. Chobanova[83], M. Chrzaszcz[41], A. Chubykin[44], V. Chulikov[28,36], P. Ciambrone[28], X. Cid Vidal[47], G. Ciezarek[49], P. Cifra[38], P.E.L. Clarke[59], M. Clemencic[49], H.V. Cliff[56], J. Closier[49], C. Cocha Toapaxi[22], V. Coco[49], J. Cogan[13], E. Cogneras[11], L. Cojocariu[43], S. Collaviti[50], P. Collins[49], T. Colombo[49], M. Colonna[19], A. Comerma-Montells[45], L. Congedo[24], A. Contu[32], N. Cooke[60], C. Coronel[66], I. Corredoira[12], A. Correia[16], G. Corti[49], J. Cottee Meldrum[55], B. Couturier[49], D.C. Craik[51], M. Cruz Torres[2,f], E. Curras Rivera[50], R. Currie[59], C.L. Da Silva[68], S. Dadabaev[44], L. Dai[71], X. Dai[4], E. Dall'Occo[49], J. Dalseno[83], C. D'Ambrosio[62],

JHEP11(2025)172

J. Daniel[11], P. d'Argent[24], G. Darze[3], A. Davidson[57], J.E. Davies[63], O. De Aguiar Francisco[63], C. De Angelis[32,j], F. De Benedetti[49], J. de Boer[38], K. De Bruyn[80], S. De Capua[63], M. De Cian[63], U. De Freitas Carneiro Da Graca[2,a], E. De Lucia[28], J.M. De Miranda[2], L. De Paula[3], M. De Serio[24,g], P. De Simone[28], F. De Vellis[19], J.A. de Vries[81], F. Debernardis[24], D. Decamp[10], S. Dekkers[1], L. Del Buono[16], B. Delaney[65], H.-P. Dembinski[19], J. Deng[8], V. Denysenko[51], O. Deschamps[11], F. Dettori[32,j], B. Dey[78], P. Di Nezza[28], I. Diachkov[44], S. Didenko[44], S. Ding[69], Y. Ding[50], L. Dittmann[22], V. Dobishuk[53], A. D. Docheva[60], C. Dong[4,b], A.M. Donohoe[23], F. Dordei[32], A.C. dos Reis[2], A. D. Dowling[69], W. Duan[72], P. Duda[82], M.W. Dudek[41], L. Dufour[49], V. Duk[34], P. Durante[49], M. M. Duras[82], J.M. Durham[68], O. D. Durmus[78], A. Dziurda[41], A. Dzyuba[44], S. Easo[58], E. Eckstein[18], U. Egede[1], A. Egorychev[44], V. Egorychev[44], S. Eisenhardt[59], E. Ejopu[63], L. Eklund[84], M. Elashri[66], J. Ellbracht[19], S. Ely[62], A. Ene[43], J. Eschle[69], S. Esen[22], T. Evans[38], F. Fabiano[32], S. Faghih[66], L.N. Falcao[2], B. Fang[7], R. Fantechi[35], L. Fantini[34,r,49], M. Faria[50], K. Farmer[59], D. Fazzini[31,o], L. Felkowski[82], M. Feng[5,7], M. Feo[19], A. Fernandez Casani[48], M. Fernandez Gomez[47], A.D. Fernez[67], F. Ferrari[25,i], F. Ferreira Rodrigues[3], M. Ferrillo[51], M. Ferro-Luzzi[49], S. Filippov[44], R.A. Fini[24], M. Fiorini[26,k], M. Firlej[40], K.L. Fischer[64], D.S. Fitzgerald[86], C. Fitzpatrick[63], T. Fiutowski[40], F. Fleuret[15], A. Fomin[52], M. Fontana[25], L. F. Foreman[63], R. Forty[49], D. Foulds-Holt[59], V. Franco Lima[3], M. Franco Sevilla[67], M. Frank[49], E. Franzoso[26,k], G. Frau[63], C. Frei[49], D.A. Friday[63], J. Fu[7], Q. Führing[19,e,56], Y. Fujii[1], T. Fulghesu[13], E. Gabriel[38], G. Galati[24], M.D. Galati[38], A. Gallas Torreira[47], D. Galli[25,i], S. Gambetta[59], M. Gandelman[3], P. Gandini[30], B. Ganie[63], H. Gao[7], R. Gao[64], T.Q. Gao[56], Y. Gao[8], Y. Gao[6], Y. Gao[8], L.M. Garcia Martin[50], P. Garcia Moreno[45], J. García Pardiñas[65], P. Gardner[67], K. G. Garg[8], L. Garrido[45], C. Gaspar[49], A. Gavrikov[33], L.L. Gerken[19], E. Gersabeck[20], M. Gersabeck[20], T. Gershon[57], S. Ghizzo[29,m], Z. Ghorbanimoghaddam[55], L. Giambastiani[33,q], F. I. Giasemis[16,d], V. Gibson[56], H.K. Giemza[42], A.L. Gilman[64], M. Giovannetti[28], A. Gioventù[45], L. Girardey[63,58], M.A. Giza[41], F.C. Glaser[14,22], V.V. Gligorov[16], C. Göbel[70], L. Golinka-Bezshyyko[85], E. Golobardes[46], D. Golubkov[44], A. Golutvin[62,49], S. Gomez Fernandez[45], W. Gomulka[40], F. Goncalves Abrantes[64], M. Goncerz[41], G. Gong[4,b], J. A. Gooding[19], I.V. Gorelov[44], C. Gotti[31], E. Govorkova[65], J.P. Grabowski[18], L.A. Granado Cardoso[49], E. Graugés[45], E. Graverini[50,t], L. Grazette[57], G. Graziani[27], A. T. Grecu[43], L.M. Greeven[38], N.A. Grieser[66], L. Grillo[60], S. Gromov[44], C. Gu[15], M. Guarise[26], L. Guerry[11], V. Guliaeva[44], P. A. Günther[22], A.-K. Guseinov[50], E. Gushchin[44], Y. Guz[6,49], T. Gys[49], K. Habermann[18], T. Hadavizadeh[1], C. Hadjivasiliou[67], G. Haefeli[50], C. Haen[49], G. Hallett[57], P.M. Hamilton[67], J. Hammerich[61], Q. Han[33], X. Han[22,49], S. Hansmann-Menzemer[22], L. Hao[7], N. Harnew[64], T. H. Harris[1], M. Hartmann[14], S. Hashmi[40], J. He[7,c], F. Hemmer[49], C. Henderson[66], R.D.L. Henderson[1], A.M. Hennequin[49], K. Hennessy[61], L. Henry[50], J. Herd[62], P. Herrero Gascon[22], J. Heuel[17], A. Hicheur[3], G. Hijano Mendizabal[51], J. Horswill[63], R. Hou[8], Y. Hou[11], N. Howarth[61], J. Hu[72], W. Hu[7], X. Hu[4,b], W. Hulsbergen[38], R.J. Hunter[57], M. Hushchyn[44], D. Hutchcroft[61], M. Idzik[40], D. Ilin[44], P. Ilten[66], A. Inglessi[44], A. Iniukhin[44], A. Ishteev[44], K. Ivshin[44], H. Jage[17],

JHEP11(2025)172

S.J. Jaimes Elles[76,49,48], S. Jakobsen[49], E. Jans[38], B.K. Jashal[48], A. Jawahery[67], V. Jevtic[19], E. Jiang[67], X. Jiang[5,7], Y. Jiang[7], Y. J. Jiang[6], M. John[64], A. John Rubesh Rajan[23], D. Johnson[54], C.R. Jones[56], T.P. Jones[57], S. Joshi[42], B. Jost[49], J. Juan Castella[56], N. Jurik[49], I. Juszczak[41], D. Kaminaris[50], S. Kandybei[52], M. Kane[59], Y. Kang[4,b], C. Kar[11], M. Karacson[49], D. Karpenkov[44], A. Kauniskangas[50], J.W. Kautz[66], M.K. Kazanecki[41], F. Keizer[49], M. Kenzie[56], T. Ketel[38], B. Khanji[69], A. Kharisova[44], S. Kholodenko[35,49], G. Khreich[14], T. Kirn[17], V.S. Kirsebom[31,o], O. Kitouni[65], S. Klaver[39], N. Kleijne[35,s], K. Klimaszewski[42], M.R. Kmiec[42], S. Koliiev[53], L. Kolk[19], A. Konoplyannikov[6], P. Kopciewicz[49], P. Koppenburg[38], A. Korchin[52], M. Korolev[44], I. Kostiuk[38], O. Kot[53], S. Kotriakhova, A. Kozachuk[44], P. Kravchenko[44], L. Kravchuk[44], M. Kreps[57], P. Krokovny[44], W. Krupa[69], W. Krzemien[42], O. Kshyvanskyi[53], S. Kubis[82], M. Kucharczyk[41], V. Kudryavtsev[44], E. Kulikova[44], A. Kupsc[84], V. Kushnir[52], B. Kutsenko[13], I. Kyryllin[52], D. Lacarrere[49], P. Laguarta Gonzalez[45], A. Lai[32], A. Lampis[32], D. Lancierini[62], C. Landesa Gomez[47], J.J. Lane[1], G. Lanfranchi[28], C. Langenbruch[22], J. Langer[19], O. Lantwin[44], T. Latham[57], F. Lazzari[35,t,49], C. Lazzeroni[54], R. Le Gac[13], H. Lee[61], R. Lefèvre[11], A. Leflat[44], S. Legotin[44], M. Lehuraux[57], E. Lemos Cid[49], O. Leroy[13], T. Lesiak[41], E. D. Lesser[49], B. Leverington[22], A. Li[4,b], C. Li[4], C. Li[13], H. Li[72], J. Li[8], K. Li[75], L. Li[63], M. Li[8], P. Li[7], P.-R. Li[73], Q. Li[5,7], S. Li[8], T. Li[71], T. Li[72], Y. Li[8], Y. Li[5], Z. Lian[4,b], X. Liang[69], S. Libralon[48], C. Lin[7], T. Lin[58], R. Lindner[49], H. Linton[62], R. Litvinov[32,49], D. Liu[8], F. L. Liu[1], G. Liu[72], K. Liu[73], S. Liu[5,7], W. Liu[8], Y. Liu[59], Y. Liu[73], Y. L. Liu[62], G. Loachamin Ordonez[70], A. Lobo Salvia[45], A. Loi[32], T. Long[56], J.H. Lopes[3], A. Lopez Huertas[45], S. López Soliño[47], Q. Lu[15], C. Lucarelli[27,l], D. Lucchesi[33,q], M. Lucio Martinez[48], Y. Luo[6], A. Lupato[33,h], E. Luppi[26,k], K. Lynch[23], X.-R. Lyu[7], G. M. Ma[4,b], S. Maccolini[19], F. Machefert[14], F. Maciuc[43], B. Mack[69], I. Mackay[64], L. M. Mackey[69], L.R. Madhan Mohan[56], M. J. Madurai[54], D. Magdalinski[38], D. Maisuzenko[44], J.J. Malczewski[41], S. Malde[64], L. Malentacca[49], A. Malinin[44], T. Maltsev[44], G. Manca[32,j], G. Mancinelli[13], C. Mancuso[14], R. Manera Escalero[45], F. M. Manganella[37], D. Manuzzi[25], D. Marangotto[30], J.F. Marchand[10], R. Marchevski[50], U. Marconi[25], E. Mariani[16], S. Mariani[49], C. Marin Benito[45], J. Marks[22], A.M. Marshall[55], L. Martel[64], G. Martelli[34], G. Martellotti[36], L. Martinazzoli[49], M. Martinelli[31,o], D. Martinez Gomez[80], D. Martinez Santos[83], F. Martinez Vidal[48], A. Martorell i Granollers[46], A. Massafferri[2], R. Matev[49], A. Mathad[49], V. Matiunin[44], C. Matteuzzi[69], K.R. Mattioli[15], A. Mauri[62], E. Maurice[15], J. Mauricio[45], P. Mayencourt[50], J. Mazorra de Cos[48], M. Mazurek[42], M. McCann[62], T.H. McGrath[63], N.T. McHugh[60], A. McNab[63], R. McNulty[23], B. Meadows[66], G. Meier[19], D. Melnychuk[42], F. M. Meng[4,b], M. Merk[38,81], A. Merli[50], L. Meyer Garcia[67], D. Miao[5,7], H. Miao[7], M. Mikhasenko[77], D.A. Milanes[76,y], A. Minotti[31,o], E. Minucci[28], T. Miralles[11], B. Mitreska[19], D.S. Mitzel[19], A. Modak[58], L. Moeser[19], R.A. Mohammed[64], R.D. Moise[17], E. F. Molina Cardenas[86], T. Mombächer[49], M. Monk[57,1], S. Monteil[11], A. Morcillo Gomez[47], G. Morello[28], M.J. Morello[35,s], M.P. Morgenthaler[22], J. Moron[40], W. Morren[38], A.B. Morris[49], A.G. Morris[13], R. Mountain[69], H. Mu[4,b], Z. M. Mu[6], E. Muhammad[57], F. Muheim[59],

JHEP11(2025)172

M. Mulder[80], K. Müller[51], F. Muñoz-Rojas[9], R. Murta[62], V. Mytrochenko[52], P. Naik[61], T. Nakada[50], R. Nandakumar[58], T. Nanut[49], I. Nasteva[3], M. Needham[59], E. Nekrasova[44], N. Neri[30,n], S. Neubert[18], N. Neufeld[49], P. Neustroev[44], J. Nicolini[49], D. Nicotra[81], E.M. Niel[15], N. Nikitin[44], Q. Niu[73], P. Nogarolli[3], P. Nogga[18], C. Normand[55], J. Novoa Fernandez[47], G. Nowak[66], C. Nunez[86], H. N. Nur[60], A. Oblakowska-Mucha[40], V. Obraztsov[44], T. Oeser[17], S. Okamura[26,k], A. Okhotnikov[44], O. Okhrimenko[53], R. Oldeman[32,j], F. Oliva[59], M. Olocco[19], C.J.G. Onderwater[81], R.H. O'Neil[49], D. Osthues[19], J.M. Otalora Goicochea[3], P. Owen[51], A. Oyanguren[48], O. Ozcelik[59], F. Paciolla[35,w], A. Padee[42], K.O. Padeken[18], B. Pagare[47], T. Pajero[49], A. Palano[24], M. Palutan[28], X. Pan[4,b], S. Panebianco[12], G. Panshin[5], L. Paolucci[57], A. Papanestis[58,49], M. Pappagallo[24,g], L.L. Pappalardo[26], C. Pappenheimer[66], C. Parkes[63], D. Parmar[77], B. Passalacqua[26,k], G. Passaleva[27], D. Passaro[35,s,49], A. Pastore[24], M. Patel[62], J. Patoc[64], C. Patrignani[25,i], A. Paul[69], C.J. Pawley[81], A. Pellegrino[38], J. Peng[5,7], M. Pepe Altarelli[28], S. Perazzini[25], D. Pereima[44], H. Pereira Da Costa[68], A. Pereiro Castro[47], P. Perret[11], A. Perrevoort[80], A. Perro[49,13], M.J. Peters[66], K. Petridis[55], A. Petrolini[29,m], J. P. Pfaller[66], H. Pham[69], L. Pica[35], M. Piccini[34], L. Piccolo[32], B. Pietrzyk[10], G. Pietrzyk[14], R. N. Pilato[61], D. Pinci[36], F. Pisani[49], M. Pizzichemi[31,o,49], V. M. Placinta[43], M. Plo Casasus[47], T. Poeschl[49], F. Polci[16], M. Poli Lener[28], A. Poluektov[13], N. Polukhina[44], I. Polyakov[63], E. Polycarpo[3], S. Ponce[49], D. Popov[7,49], S. Poslavskii[44], K. Prasanth[59], C. Prouve[83], D. Provenzano[32,j], V. Pugatch[53], G. Punzi[35,t], S. Qasim[51], Q. Q. Qian[6], W. Qian[7], N. Qin[4,b], S. Qu[4,b], R. Quagliani[49], R.I. Rabadan Trejo[57], J.H. Rademacker[55], M. Rama[35], M. Ramírez García[86], V. Ramos De Oliveira[70], M. Ramos Pernas[57], M.S. Rangel[3], F. Ratnikov[44], G. Raven[39], M. Rebollo De Miguel[48], F. Redi[30,h], J. Reich[55], F. Reiss[20], Z. Ren[7], P.K. Resmi[64], M. Ribalda Galvez[45], R. Ribatti[50], G. Ricart[15,12], D. Riccardi[35,s], S. Ricciardi[58], K. Richardson[65], M. Richardson-Slipper[59], K. Rinnert[61], P. Robbe[14,49], G. Robertson[60], E. Rodrigues[61], A. Rodriguez Alvarez[45], E. Rodriguez Fernandez[47], J.A. Rodriguez Lopez[76], E. Rodriguez Rodriguez[49], J. Roensch[19], A. Rogachev[44], A. Rogovskiy[58], D.L. Rolf[19], P. Roloff[49], V. Romanovskiy[66], A. Romero Vidal[47], G. Romolini[26], F. Ronchetti[50], T. Rong[6], M. Rotondo[28], S. R. Roy[22], M.S. Rudolph[69], M. Ruiz Diaz[22], R.A. Ruiz Fernandez[47], J. Ruiz Vidal[81], J. J. Saavedra-Arias[9], J.J. Saborido Silva[47], R. Sadek[15], N. Sagidova[44], D. Sahoo[78], N. Sahoo[54], B. Saitta[32,j], M. Salomoni[31,49,o], I. Sanderswood[48], R. Santacesaria[36], C. Santamarina Rios[47], M. Santimaria[28], L. Santoro[2], E. Santovetti[37], A. Saputi[26,49], D. Saranin[44], A. Sarnatskiy[80], G. Sarpis[59], M. Sarpis[79], C. Satriano[36,u], A. Satta[37], M. Saur[73], D. Savrina[44], H. Sazak[17], F. Sborzacchi[49,28], A. Scarabotto[19], S. Schael[17], S. Scherl[61], M. Schiller[22], H. Schindler[49], M. Schmelling[21], B. Schmidt[49], S. Schmitt[17], H. Schmitz[18], O. Schneider[50], A. Schopper[62], N. Schulte[19], S. Schulte[50], M.H. Schune[14], G. Schwering[17], B. Sciascia[28], A. Sciuccati[49], I. Segal[77], S. Sellam[47], A. Semennikov[44], T. Senger[51], M. Senghi Soares[39], A. Sergi[29,m], N. Serra[51], L. Sestini[27], A. Seuthe[19], B. Sevilla Sanjuan[46], Y. Shang[6], D.M. Shangase[86], M. Shapkin[44], R. S. Sharma[69], I. Shchemerov[44], L. Shchutska[50], T. Shears[61], L. Shekhtman[44], Z. Shen[38], S. Sheng[5,7], V. Shevchenko[44], B. Shi[7], Q. Shi[7], Y. Shimizu[14], E. Shmanin[25], R. Shorkin[44],

JHEP11(2025)172

J.D. Shupperd[69], R. Silva Coutinho[69], G. Simi[33,q], S. Simone[24,g], M. Singha[78], N. Skidmore[57], T. Skwarnicki[69], M.W. Slater[54], E. Smith[65], K. Smith[68], M. Smith[62], L. Soares Lavra[59], M.D. Sokoloff[66], F.J.P. Soler[60], A. Solomin[55], A. Solovev[44], I. Solovyev[44], N. S. Sommerfeld[18], R. Song[1], Y. Song[50], Y. Song[4,b], Y. S. Song[6], F.L. Souza De Almeida[69], B. Souza De Paula[3], E. Spadaro Norella[29,m], E. Spedicato[25], J.G. Speer[19], E. Spiridenkov[44], P. Spradlin[60], V. Sriskaran[49], F. Stagni[49], M. Stahl[77], S. Stahl[49], S. Stanislaus[64], M. Stefaniak[87], E.N. Stein[49], O. Steinkamp[51], O. Stenyakin[44], H. Stevens[19], D. Strekalina[44], Y. Su[7], F. Suljik[64], J. Sun[32], L. Sun[74], D. Sundfeld[2], W. Sutcliffe[51], K. Swientek[40], F. Swystun[56], A. Szabelski[42], T. Szumlak[40], Y. Tan[4,b], Y. Tang[74], Y. T. Tang[7], M.D. Tat[22], A. Terentev[44], F. Terzuoli[35,w,49], F. Teubert[49], E. Thomas[49], D.J.D. Thompson[54], H. Tilquin[62], V. Tisserand[11], S. T'Jampens[10], M. Tobin[5], L. Tomassetti[26,k], G. Tonani[30], X. Tong[6], T. Tork[30], D. Torres Machado[2], L. Toscano[19], D.Y. Tou[4,b], C. Trippl[46], G. Tuci[22], N. Tuning[38], L.H. Uecker[22], A. Ukleja[40], D.J. Unverzagt[22], A. Upadhyay[49], B. Urbach[59], A. Usachov[39], A. Ustyuzhanin[44], U. Uwer[22], V. Vagnoni[25], V. Valcarce Cadenas[47], G. Valenti[25], N. Valls Canudas[49], J. van Eldik[49], H. Van Hecke[68], E. van Herwijnen[62], C.B. Van Hulse[47,z], R. Van Laak[50], M. van Veghel[38], G. Vasquez[51], R. Vazquez Gomez[45], P. Vazquez Regueiro[47], C. Vázquez Sierra[83], S. Vecchi[26], J.J. Velthuis[55], M. Veltri[27,x], A. Venkateswaran[50], M. Verdoglia[32], M. Vesterinen[57], D. Vico Benet[64], P. Vidrier Villalba[45], M. Vieites Diaz[47], X. Vilasis-Cardona[46], E. Vilella Figueras[61], A. Villa[25], P. Vincent[16], B. Vivacqua[3], F.C. Volle[54], D. vom Bruch[13], N. Voropaev[44], K. Vos[81], C. Vrahas[59], J. Wagner[19], J. Walsh[35], E.J. Walton[1,57], G. Wan[6], A. Wang[7], C. Wang[22], G. Wang[8], H. Wang[73], J. Wang[6], J. Wang[5], J. Wang[4,b], J. Wang[74], M. Wang[49], N. W. Wang[7], R. Wang[55], X. Wang[8], X. Wang[72], X. W. Wang[62], Y. Wang[75], Y. Wang[6], Y. W. Wang[73], Z. Wang[14], Z. Wang[4,b], Z. Wang[30], J.A. Ward[57,1], M. Waterlaat[49], N.K. Watson[54], D. Websdale[62], Y. Wei[6], J. Wendel[83], B.D.C. Westhenry[55], C. White[56], M. Whitehead[60], E. Whiter[54], A.R. Wiederhold[63], D. Wiedner[19], G. Wilkinson[64,49], M.K. Wilkinson[66], M. Williams[65], M. J. Williams[49], M.R.J. Williams[59], R. Williams[56], Z. Williams[55], F.F. Wilson[58], M. Winn[12], W. Wislicki[42], M. Witek[41], L. Witola[19], G. Wormser[14], S.A. Wotton[56], H. Wu[69], J. Wu[8], X. Wu[74], Y. Wu[6,56], Z. Wu[7], K. Wyllie[49], S. Xian[72], Z. Xiang[5], Y. Xie[8], T. X. Xing[30], A. Xu[35,s], L. Xu[4,b], L. Xu[4,b], M. Xu[49], Z. Xu[49], Z. Xu[7], Z. Xu[5], K. Yang[62], X. Yang[6], Y. Yang[29], Z. Yang[6], V. Yeroshenko[14], H. Yeung[63], H. Yin[8], X. Yin[7], C. Y. Yu[6], J. Yu[71], X. Yuan[5], Y Yuan[5,7], E. Zaffaroni[50], M. Zavertyaev[21], M. Zdybal[41], F. Zenesini[25], C. Zeng[5,7], M. Zeng[4,b], C. Zhang[6], D. Zhang[8], J. Zhang[7], L. Zhang[4,b], R. Zhang[8], S. Zhang[71], S. Zhang[64], Y. Zhang[6], Y. Z. Zhang[4,b], Z. Zhang[4,b], Y. Zhao[22], A. Zhelezov[22], S. Z. Zheng[6], X. Z. Zheng[4,b], Y. Zheng[7], T. Zhou[6], X. Zhou[8], Y. Zhou[7], V. Zhovkovska[57], L. Z. Zhu[7], X. Zhu[4,b], X. Zhu[8], Y. Zhu[17], V. Zhukov[17], J. Zhuo[48], Q. Zou[5,7], D. Zuliani[33,q], G. Zunica[50]

[1] *School of Physics and Astronomy, Monash University, Melbourne, Australia*
[2] *Centro Brasileiro de Pesquisas Físicas (CBPF), Rio de Janeiro, Brazil*
[3] *Universidade Federal do Rio de Janeiro (UFRJ), Rio de Janeiro, Brazil*
[4] *Department of Engineering Physics, Tsinghua University, Beijing, China*
[5] *Institute Of High Energy Physics (IHEP), Beijing, China*

JHEP11(2025)172

[6] School of Physics State Key Laboratory of Nuclear Physics and Technology, Peking University, Beijing, China
[7] University of Chinese Academy of Sciences, Beijing, China
[8] Institute of Particle Physics, Central China Normal University, Wuhan, Hubei, China
[9] Consejo Nacional de Rectores (CONARE), San Jose, Costa Rica
[10] Université Savoie Mont Blanc, CNRS, IN2P3-LAPP, Annecy, France
[11] Université Clermont Auvergne, CNRS/IN2P3, LPC, Clermont-Ferrand, France
[12] Université Paris-Saclay, Centre d'Etudes de Saclay (CEA), IRFU, Saclay, France, Gif-Sur-Yvette, France
[13] Aix Marseille Univ, CNRS/IN2P3, CPPM, Marseille, France
[14] Université Paris-Saclay, CNRS/IN2P3, IJCLab, Orsay, France
[15] Laboratoire Leprince-Ringuet, CNRS/IN2P3, Ecole Polytechnique, Institut Polytechnique de Paris, Palaiseau, France
[16] LPNHE, Sorbonne Université, Paris Diderot Sorbonne Paris Cité, CNRS/IN2P3, Paris, France
[17] I. Physikalisches Institut, RWTH Aachen University, Aachen, Germany
[18] Universität Bonn — Helmholtz-Institut für Strahlen und Kernphysik, Bonn, Germany
[19] Fakultät Physik, Technische Universität Dortmund, Dortmund, Germany
[20] Physikalisches Institut, Albert-Ludwigs-Universität Freiburg, Freiburg, Germany
[21] Max-Planck-Institut für Kernphysik (MPIK), Heidelberg, Germany
[22] Physikalisches Institut, Ruprecht-Karls-Universität Heidelberg, Heidelberg, Germany
[23] School of Physics, University College Dublin, Dublin, Ireland
[24] INFN Sezione di Bari, Bari, Italy
[25] INFN Sezione di Bologna, Bologna, Italy
[26] INFN Sezione di Ferrara, Ferrara, Italy
[27] INFN Sezione di Firenze, Firenze, Italy
[28] INFN Laboratori Nazionali di Frascati, Frascati, Italy
[29] INFN Sezione di Genova, Genova, Italy
[30] INFN Sezione di Milano, Milano, Italy
[31] INFN Sezione di Milano-Bicocca, Milano, Italy
[32] INFN Sezione di Cagliari, Monserrato, Italy
[33] INFN Sezione di Padova, Padova, Italy
[34] INFN Sezione di Perugia, Perugia, Italy
[35] INFN Sezione di Pisa, Pisa, Italy
[36] INFN Sezione di Roma La Sapienza, Roma, Italy
[37] INFN Sezione di Roma Tor Vergata, Roma, Italy
[38] Nikhef National Institute for Subatomic Physics, Amsterdam, Netherlands
[39] Nikhef National Institute for Subatomic Physics and VU University Amsterdam, Amsterdam, Netherlands
[40] AGH — University of Krakow, Faculty of Physics and Applied Computer Science, Kraków, Poland
[41] Henryk Niewodniczanski Institute of Nuclear Physics Polish Academy of Sciences, Kraków, Poland
[42] National Center for Nuclear Research (NCBJ), Warsaw, Poland
[43] Horia Hulubei National Institute of Physics and Nuclear Engineering, Bucharest-Magurele, Romania
[44] Authors affiliated with an institute formerly covered by a cooperation agreement with CERN.
[45] ICCUB, Universitat de Barcelona, Barcelona, Spain
[46] La Salle, Universitat Ramon Llull, Barcelona, Spain
[47] Instituto Galego de Física de Altas Enerxías (IGFAE), Universidade de Santiago de Compostela, Santiago de Compostela, Spain
[48] Instituto de Fisica Corpuscular, Centro Mixto Universidad de Valencia — CSIC, Valencia, Spain
[49] European Organization for Nuclear Research (CERN), Geneva, Switzerland
[50] Institute of Physics, Ecole Polytechnique Fédérale de Lausanne (EPFL), Lausanne, Switzerland
[51] Physik-Institut, Universität Zürich, Zürich, Switzerland
[52] NSC Kharkiv Institute of Physics and Technology (NSC KIPT), Kharkiv, Ukraine
[53] Institute for Nuclear Research of the National Academy of Sciences (KINR), Kyiv, Ukraine
[54] School of Physics and Astronomy, University of Birmingham, Birmingham, United Kingdom
[55] H.H. Wills Physics Laboratory, University of Bristol, Bristol, United Kingdom

JHEP11(2025)172

[56] Cavendish Laboratory, University of Cambridge, Cambridge, United Kingdom
[57] Department of Physics, University of Warwick, Coventry, United Kingdom
[58] STFC Rutherford Appleton Laboratory, Didcot, United Kingdom
[59] School of Physics and Astronomy, University of Edinburgh, Edinburgh, United Kingdom
[60] School of Physics and Astronomy, University of Glasgow, Glasgow, United Kingdom
[61] Oliver Lodge Laboratory, University of Liverpool, Liverpool, United Kingdom
[62] Imperial College London, London, United Kingdom
[63] Department of Physics and Astronomy, University of Manchester, Manchester, United Kingdom
[64] Department of Physics, University of Oxford, Oxford, United Kingdom
[65] Massachusetts Institute of Technology, Cambridge, MA, United States
[66] University of Cincinnati, Cincinnati, OH, United States
[67] University of Maryland, College Park, MD, United States
[68] Los Alamos National Laboratory (LANL), Los Alamos, NM, United States
[69] Syracuse University, Syracuse, NY, United States
[70] Pontifícia Universidade Católica do Rio de Janeiro (PUC-Rio), Rio de Janeiro, Brazil, associated to [3]
[71] School of Physics and Electronics, Hunan University, Changsha City, China, associated to [8]
[72] Guangdong Provincial Key Laboratory of Nuclear Science, Guangdong-Hong Kong Joint Laboratory of Quantum Matter, Institute of Quantum Matter, South China Normal University, Guangzhou, China, associated to [4]
[73] Lanzhou University, Lanzhou, China, associated to [5]
[74] School of Physics and Technology, Wuhan University, Wuhan, China, associated to [4]
[75] Henan Normal University, Xinxiang, China, associated to [8]
[76] Departamento de Fisica, Universidad Nacional de Colombia, Bogota, Colombia, associated to [16]
[77] Ruhr Universitaet Bochum, Fakultaet f. Physik und Astronomie, Bochum, Germany, associated to [19]
[78] Eotvos Lorand University, Budapest, Hungary, associated to [49]
[79] Faculty of Physics, Vilnius University, Vilnius, Lithuania, associated to [20]
[80] Van Swinderen Institute, University of Groningen, Groningen, Netherlands, associated to [38]
[81] Universiteit Maastricht, Maastricht, Netherlands, associated to [38]
[82] Tadeusz Kosciuszko Cracow University of Technology, Cracow, Poland, associated to [41]
[83] Universidade da Coruña, A Coruña, Spain, associated to [46]
[84] Department of Physics and Astronomy, Uppsala University, Uppsala, Sweden, associated to [60]
[85] Taras Schevchenko University of Kyiv, Faculty of Physics, Kyiv, Ukraine, associated to [14]
[86] University of Michigan, Ann Arbor, MI, United States, associated to [69]
[87] Ohio State University, Columbus, United States, associated to [68]

[a] Centro Federal de Educacão Tecnológica Celso Suckow da Fonseca, Rio De Janeiro, Brazil
[b] Center for High Energy Physics, Tsinghua University, Beijing, China
[c] Hangzhou Institute for Advanced Study, UCAS, Hangzhou, China
[d] LIP6, Sorbonne Université, Paris, France
[e] Lamarr Institute for Machine Learning and Artificial Intelligence, Dortmund, Germany
[f] Universidad Nacional Autónoma de Honduras, Tegucigalpa, Honduras
[g] Università di Bari, Bari, Italy
[h] Università di Bergamo, Bergamo, Italy
[i] Università di Bologna, Bologna, Italy
[j] Università di Cagliari, Cagliari, Italy
[k] Università di Ferrara, Ferrara, Italy
[l] Università di Firenze, Firenze, Italy
[m] Università di Genova, Genova, Italy
[n] Università degli Studi di Milano, Milano, Italy
[o] Università degli Studi di Milano-Bicocca, Milano, Italy
[p] Università di Modena e Reggio Emilia, Modena, Italy
[q] Università di Padova, Padova, Italy
[r] Università di Perugia, Perugia, Italy
[s] Scuola Normale Superiore, Pisa, Italy

JHEP11(2025)172

[t] Università di Pisa, Pisa, Italy
[u] Università della Basilicata, Potenza, Italy
[v] Università di Roma Tor Vergata, Roma, Italy
[w] Università di Siena, Siena, Italy
[x] Università di Urbino, Urbino, Italy
[y] Universidad de Ingeniería y Tecnología (UTEC), Lima, Peru
[z] Universidad de Alcalá, Alcalá de Henares, Spain
[aa] Facultad de Ciencias Fisicas, Madrid, Spain
[†] Deceased

JHEP11(2025)172